# Ab Initio MO Study of the Full Catalytic Cycle of Olefin Hydrogenation by the Wilkinson Catalyst $RhCl(PR_3)_3$

**C. Daniel,[†,§] N. Koga,[†] J. Han,[‡] X. Y. Fu,[‡] and K. Morokuma*,[†]**

*Contribution from the Institute for Molecular Science, Myodaiji, Okazaki 444, Japan, and the Department of Chemistry, Beijing Normal University, Beijing, China.*
*Received September 23, 1987*

**Abstract:** The potential energy profile for the full catalytic cycle of olefin hydrogenation by the Wilkinson catalyst has been studied with the ab initio MO method. The geometries of the transition states as well as the intermediates have been determined with the RHF energy gradient method for each step of the model Halpern mechanism, i.e., (i) the oxidative addition of $H_2$ to $RhCl(PR_3)_2$, (ii) the olefin coordination to $H_2RhCl(PR_3)_2$, (iii) the intramolecular olefin migratory insertion of $H_2RhCl(PR_3)_2(C_2H_4)$, (iv) the isomerization of *trans*-$HRhCl(PR_3)_2(C_2H_5)$, and (v) the reductive elimination of $C_2H_6$ from *cis*-$HRhCl(PR_3)_2(C_2H_5)$ to regenerate $RhCl(PR_3)_2$. The energetics for some critical steps has been calculated also with the second-order Møller–Plesset perturbation theory. The first two steps, exothermic without significant barrier, should take place easily. The olefin migratory insertion has a high barrier. The resultant trans hydride alkyl complex isomerizes with a small barrier very exothermically to give a cis complex. The olefin insertion combined with the first portion of isomerization constitutes the rate-determining step. The nearly thermoneutral reductive elimination of $C_2H_6$ takes place with a modest barrier. The overall potential energy profile is smooth without excessive barriers and without too stable intermediates. The geometries and the energetics of the intermediates and the transition states have been discussed in detail. The potential energy profiles of some elementary reactions have been compared with those of other transition-metal complexes, and factors controlling the potential features have been discussed. For instance, the Pt analogue is not a good catalyst where the $\beta$-hydrogen elimination takes place easily and the $C_2H_6$ reductive elimination has a high barrier. A large cis chloride effect as well as the trans hydride effect plays an important role in determining the potential profiles.

## I. Introduction

There have been known many catalytic processes which involve elementary reactions of organometallic compounds.[1] One of the most extensively studied is the homogeneous hydrogenation of olefins by the chlorotris(triphenylphosphine)rhodium(I) complex (the so-called Wilkinson catalyst) $RhCl(PPh_3)_3$.[2-7] The most commonly accepted mechanism of this catalytic process is due to Halpern, supported by careful kinetic[2-6] and spectroscopic[7] studies. This mechanism is outlined in Scheme I, where the route dominating the catalytic cycle is surrounded by the dotted circle. According to this scheme, the predominant hydride route constitutes an oxidative addition of hydrogen molecule prior to olefin coordination. Both the associative pathway through $RhCl(PPh_3)_3$ and the dissociative pathway through $RhCl(PPh_3)_2$ could operate for hydrogenation, depending on the concentration of free $PPh_3$. But $RhCl(PPh_3)_2$ reacts with $H_2$ at least $10^4$ times faster than $RhCl(PPh_3)_3$[3b,7b] and is likely to be an active intermediate. An octahedral dihydride olefin complex $H_2RhCl(PPh_3)_2$(olefin) is the key intermediate of the catalytic cycle. The intramolecular olefin insertion reaction of this complex giving the alkyl hydride intermediate $HRhCl(PPh_3)_2$(alkyl) is generally believed to be the rate-determining step of the whole process.[3c,4,6,8] The reductive elimination of alkane from this alkyl hydride complex to regenerate $RhCl(PPh_3)_2$ is suggested to be fast, by the high stereoselectivity and the absence of olefin rearrangements and hydrogen scrambling. Within the catalytic system, five rhodium complexes have been directly observed and characterized: $H_2RhCl(PPh_3)_3$, $RhCl(PPh_3)_3$, $RhCl(PPh_3)_2$(olefin), $Rh_2Cl_2(PPh_3)_4$, and $H_2Rh_2Cl_2(PPh_3)_4$.[3b,d] However, Halpern's kinetic studies reveal that none of these complexes is directly involved in the kinetically significant catalytic cycle (contained within the dotted circle in Scheme I).[9] These stable species may be seen as labile "reservoirs" for catalytic intermediates which usually do not accumulate in sufficient concentrations to be detected. It is also known that the replacement of phenyl group in phosphine by alkyl group (for instance $P(C_2H_5)_3$) makes catalytic activity less efficient[2c] and that only the substituted olefins have been hydrogenated.

**Scheme I**

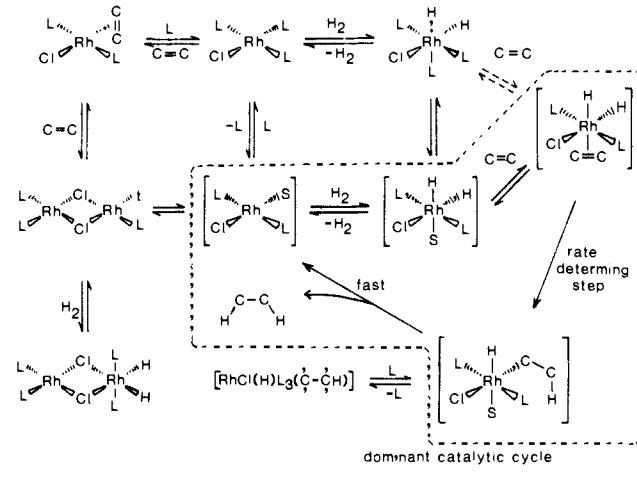


A recent detailed theoretical analysis[10] by Dedieu of the geometry and electronic structure of the possible intermediates

[†] Institute for Molecular Science.
[‡] Beijing Normal University.
[§] Permanent Address: Laboratoire de Chimie Quantique, Institut Le Bel, Universite Louis Pasteur, 4, Rue Blaise Pascal, F-67000 Strasbourg, France.

(1) (a) Taqui Khan, M. M.; Martell, A. E. *Homogeneous Catalysis by Metal Complexes*; Academic: New York, 1974; Vol. I and II. (b) Kochi, J. K. *Organometallic Mechanisms and Catalysis*; Academic: New York, 1978. (c) Nakamura, A.; Tsutsui, M. *Principles and Application of Homogeneous Catalysis*; John Wiley & Sons: New York, 1980. (d) Parshall, G. W. *Homogeneous Catalysis*; John Wiley & Sons: New York, 1980.
(2) (a) Osborn, J. A.; Jardine, F. H.; Young, J. F.; Wilkinson, G. *J. Chem. Soc. A* **1966**, 1711. (b) Jardine, F. H.; Osborn, J. A.; Wilkinson, G. *J. Chem. Soc. A* **1967**, 1574. (c) Montelatici, S.; van der Ent, A.; Osborn, J. A.; Wilkinson, G. *J. Chem. Soc. A* **1968**, 1054.
(3) (a) Halpern, J. *Organotransition Metal Chemistry*; Ishii, Y., Tsutsui, M., Eds.; Plenum: New York, 1975; p 109. (b) Halpern, J.; Wong, C. S. *J. Chem. Soc., Chem. Commun.* **1973**, 629. (c) Halpern, J.; Okamoto, T.; Zakhariev, A. *J. Mol. Catal.* **1976**, *2*, 65. (d) Halpern, J. *Trans. Am. Crystallogr. Assoc.* **1978**, *14*, 59. (e) Halpern, J. *Inorg. Chim. Acta* **1981**, *50*, 11. (f) Halpern, J.; Okamoto, T. *Inorg. Chim. Acta* **1984**, *89*, L53-L54.
(4) Ohtani, Y.; Fujimoto, M.; Yamagishi, A. *Bull. Chem. Soc. Jpn.* (a) **1976**, *49*, 1871; (b) **1977**, *50*, 1453; (c) **1979**, *52*, 69.
(5) Rousseau, C.; Evrard, M.; Petit, F. *J. Mol. Catal.* **1978**, *3*, 309; **1979**, *5*, 163.
(6) Siegel, S.; Ohrt, D. *Inorg. Nucl. Chem. Lett.* **1972**, *8*, 15.
(7) (a) Meakin, P.; Jesson, J. P.; Tolman, C. A. *J. Am. Chem. Soc.* **1972**, *94*, 3240. (b) Tolman, C. A.; Meakin, P. Z.; Lindner, D. L.; Jesson, J. P. *J. Am. Chem. Soc.* **1974**, *96*, 2762.

0002-7863/88/1510-3773$01.50/0 © 1988 American Chemical Society

involved in this catalytic cycle has contributed to the understanding of the mechanism. With some limited geometry optimization, several probable stereoisomers for each intermediate have been compared for their energies. Furthermore, the reaction coordinate for olefin insertion has been followed with selected degrees of freedom.

In the last decade, the energy gradient method in the ab initio molecular orbital theory has made it possible to determine the geometry of reactants, intermediates, and transition states by fully optimizing all the geometrical parameters, and potential energy profiles of many important elementary reactions have been calculated.[11] It is only in the last few years that the method has been applied with success to elementary organometallic reactions. Those reactions thus studied include oxidative addition/reductive elimination,[12] olefin insertion/$\beta$-elimination,[13] carbonyl insertion,[14] thermolysis of ketene complexes,[15] and isomerization of metallacycle to an alkylidene–olefin complex.[16] Unique features of fully optimized molecular structures involving agostic interactions have also been discussed.[17] Despite the success of such theoretical studies of elementary organometallic reactions, the study of a full cycle of homogeneous catalytic process, consisting of several elementary reactions, has remained to be a challenge to theoreticians. We have recently reported a preliminary account of the present work as the first ab initio study of the potential energy profile of a full catalytic cycle.[18]

We concentrate on the dominant catalytic cycle of the Halpern mechanism of the olefin hydrogenation by the Wilkinson catalyst (within the dotted circle of Scheme I) and optimize with the ab initio gradient method the structures of nearly all the intermediates and transition states to determine the potential energy profile of the whole catalytic cycle. The elementary reaction steps we have studied are as follows.

(i) The oxidative addition of $H_2$ to $RhCl(PH_3)_2$

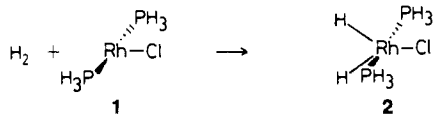

1 2

(ii) The coordination of ethylene to $H_2RhCl(PH_3)_2$

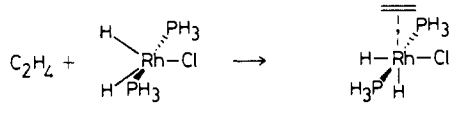

2 3

(iii) The intramolecular migratory olefin insertion to give *trans*-ethyl hydride complex, followed by isomerization to the *cis*-ethyl hydride complex

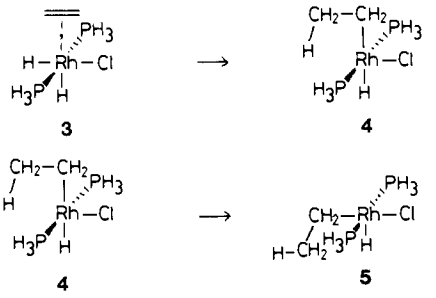

3 4 4 5

(iv) The reductive elimination of ethane from the *cis*-ethyl hydride complex

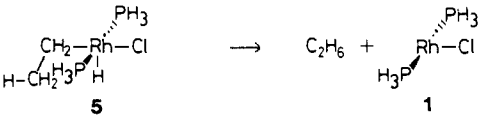

5 1

We use $PH_3$ in place of the actual ligand $PPh_3$, and $C_2H_4$ and $C_2H_5$ as models for the olefin and alkyl ligands, respectively. As discussed in a preceding paragraph, we are aware of the facts that triphenylphosphine ($PPh_3$) is the only phosphine that makes the catalytic cycle work efficiently and that ethylene does not undergo hydrogenation. However, as the first of this kind of studies, we are forced to use $PH_3$ and $C_2H_4$ for computational limitation. The role of $PPh_3$ and substituents on olefins will have to be left for a future study. The size of the bulky phosphine ligands, however, will be taken into account qualitatively in this paper in the exploration of potential energy profile. As is shown in Scheme I, the Halpern mechanism invokes solvent (S) participation in low coordinate intermediates. As the first study of the process, we completely neglect the effect of solvent in the present paper. A study including solvent effect is in progress and will be reported elsewhere in the future.

Our goals are the following: (i) to determine the fully optimized geometrical structures of the intermediates, (ii) to determine the fully optimized geometrical structures of (nearly) all the transition states connecting them, (iii) to determine the energies of the species involved, to draw the potential energy profile of the entire process, and to identify the rate-determining step, and (iv) to elucidate factors that control the features of the potential energy surface.

Section II presents a brief discussion of the method used. Sections III to VII will give results and brief discussions on each elementary reaction: the $H_2$ addition (Section III), the olefin coordination (Section IV), the olefin insertion (Section V), the isomerization (Section VI), and the ethane reductive elimination (Section VII). Summarizing the results of Sections III–VII, Section VIII focuses on the reaction mechanism of the full catalytic cycle. In Section IX we will discuss Y- and T-shaped structures and also compare the potential energy characteristics between the present Rh reactions with previously studied Pt and Pd reactions. Section X will be brief concluding remarks.

## II. Methods of Calculation

All the geometrical parameters of the intermediates as well as the transition states were optimized with the energy gradient technique[19] at the restricted Hartree–Fock (RHF) level under the effective core potential (ECP) approximation. The calculations of all the intermediates and most transition states were performed under $C_s$ symmetry, since such an assumption seemed reasonable for the structures involved. Calculations without $C_s$ restriction will be mentioned explicitly. Except for **2**, **6**, and **7** which are fully optimized, the free rotation of the $PH_3$ group around the metal–phosphorus bond was frozen at one of the HPRhCl dihedral angles of 90°. The reason why the $PH_3$ rotation is not frozen in the **2**, **6**, and **7** is that this rotation affects their optimized structures. We assumed the closed-shell singlet ground electronic state, since the

(8) However it has been also claimed that the formation of the dihydride olefinic intermediate is the rate-determining step: De Croon, M. H. J. M.; van Nisselrooij, P. F. M. T.; Kuipers, H. J. A. M.; Coenen, J. W. E. *J. Mol. Catal.* **1978**, *4*, 325.

(9) Collman, J. P.; Hegedus, L. S. *Principles and Applications of Organotransition Metal Chemistry*; Aidan Kelly, Ed.; University Science Books: Mill Valley, 1980; p 334.

(10) (a) Dedieu, A. *Inorg. Chem.* **1980**, *19*, 375. (b) Dedieu, A. *Ibid.* **1981**, *20*, 2803. (c) Dedieu, A.; Strich, A. *Ibid.* **1979**, *18*, 2940. (d) Dedieu, A.; Strich, A.; Rossi, A. *Quantum Theory of Chemical Reactions*; Daudel et al., Eds.; Reidel: Dordrecht, 1980; Vol. II, pp 193–211.

(11) Morokuma, K.; Kato, S.; Kitaura, K.; Obara, S.; Ohta, K.; Hanamura, M. *New Horizons of Quantum Chemistry*; Löwdin, P.-O., Pullmann, B., Eds.; Reidel: Dordrecht, 1983; p 221.

(12) (a) Kitaura, K.; Obara, S.; Morokuma, K. *J. Am. Chem. Soc.* **1981**, *103*, 2891. (b) Obara, S.; Kitaura, K.; Morokuma, K. *J. Am. Chem. Soc.* **1984**, *106*, 7482. (c) Low, J. J.; Goddard, W. A., III *J. Am. Chem. Soc.* **1984**, *106*, 6928. (d) Low, J. J.; Goddard, W. A., III *Organometallics* **1986**, *5*, 609. (e) Low, J. J.; Goddard, W. A., III *J. Am. Chem. Soc.* **1986**, *108*, 6115.

(13) (a) Koga, N.; Obara, S.; Kitaura, K.; Morokuma, K. *J. Am. Chem. Soc.* **1985**, *107*, 7109. (b) Koga, N.; Morokuma, K. *Quantum Chemistry: The Challenge of Transition Metals and Coordination Chemistry*; Veillard, A., Ed.; Reidel: Dordrecht, 1986; NATO ASI Series C, Vol. 176.

(14) (a) Sakaki, S.; Kitaura, K.; Morokuma, K.; Ohkubo, K. *J. Am. Chem. Soc.* **1983**, *105*, 2280. (b) Koga, N.; Morokuma, K. *J. Am. Chem. Soc.* **1985**, *107*, 7230. (c) Koga, N.; Morokuma, K. *J. Am. Chem. Soc.* **1986**, *108*, 6136.

(15) Nakamura, S.; Morokuma, K. *Organometallics*, in press.

(16) Upton, T. H.; Rappé, A. K. *J. Am. Chem. Soc.* **1985**, *107*, 1206.

(17) (a) Koga, N.; Obara, S.; Morokuma, K. *J. Am. Chem. Soc.* **1984**, *106*, 4625. (b) Obara, S.; Koga, N.; Morokuma, K. *J. Organomet. Chem.* **1984**, *270*, C33.

(18) Koga, N.; Daniel, C.; Han, J.; Fu, X. Y.; Morokuma, K. *J. Am. Chem. Soc.* **1987**, *109*, 3455.

(19) Kitaura, K.; Obara, S.; Morokuma, K. *Chem. Phys. Lett.* **1981**, *77*, 452.

**Scheme II**

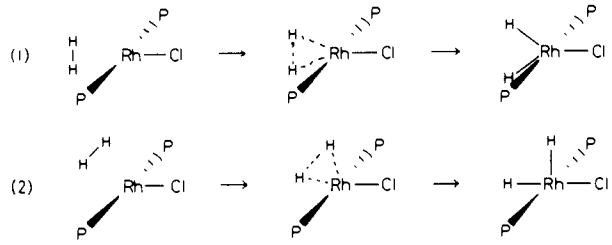

**Table I.** Calculated Relative HF Energy (kcal/mol) for the Reaction $RhCl(PH_3)_2 + H_2 \rightarrow H_2RhCl(PH_3)_2$

| $RhCl(Ph_3)_2$ (1) + $H_2$ | $H_2$–reactant complex 6 | transition state 7 | $H_2RhCl(PH_3)_2$ (2) |
|---|---|---|---|
| −1123.21336[a,b] | −20.1 | −19.5 | −26.4 |

[a] The total energy of **1** in hartrees. The reference of the relative energy is **1** + $H_2$. [b] As discussed in Section II, the structure of **1** is optimized with the frozen rotation around the M–P bonds. The fully optimized structure has an energy 0.8 kcal/mol lower than this value.

presence of strong ligands, two phosphines and a chloride, would guarantee the closed-shell nature of electronic structure.

We used the programs GAUSSIAN80 and GAUSSIAN82[20] and the following Gaussian basis sets (later referred to as the basis I): a valence double-$\zeta$ (3s,3p,4d)/[2s,2p,2d] set[21] for the rhodium atom, the 3-21G set[22] for hydrides and the ethyl group, and the STO-2G set[23] for the spectator ligands Cl and $PH_3$. The relativistic ECP obtained by Hay and Wadt[21] was used to replace core (up to 4p) electrons for the metal center Rh. In addition, the frozen-core second-order Møller–Plesset (MP2) calculations were carried out at the optimized geometries for the rate-determining step with the following larger basis sets (referred to later as the basis II): an uncontracted valence (3s,3p,4d) set for Rh,[21] the 4-31G set[24] for the ethyl group, a (10s,7p)/[3s,2p][25] triple-$\zeta$ set for the third row atoms P and Cl, and a (4s)/[3s][26] triple-$\zeta$ for the hydrides.

## III. Oxidative Addition of $H_2$ to $RhCl(PH_3)_2$

Oxidative addition of $H_2$ to low-valent transition-metal complexes is a concerted process leading to a cis adduct.[27] Previous theoretical studies of the oxidative addition of $H_2$ to the four-coordinate complex $RhCl(PH_3)_3$[10] and to the two-coordinate complex $Pt(PH_3)_2$[12b] have pointed out that the cleavage of the H–H bond in the early stage of reaction is promoted by a donative interaction from the $\sigma$ orbital of $H_2$ to a vacant metal p orbital, this interaction being enhanced by bending the phosphine ligands away from the P–M–P linearity. In the later stage of reaction where the two M–H bonds are formed, the $\pi$ back-donative interaction from a metal d orbital to the $H_2$ $\sigma^*$ orbital plays an important role.[12b] The low activation barrier calculated for Pt[12b] has shown that the oxidative addition takes place easily, in accord with the experimental findings.[28]

In our investigation of the oxidative addition of $H_2$ to the 14-electron three-coordinate intermediate **1**, we have considered two possible pathways depicted in Scheme II. We have excluded the third possibility, the attack of $H_2$ within the PRh(Cl)P plane, since this path is obviously sterically unfavorable yielding a

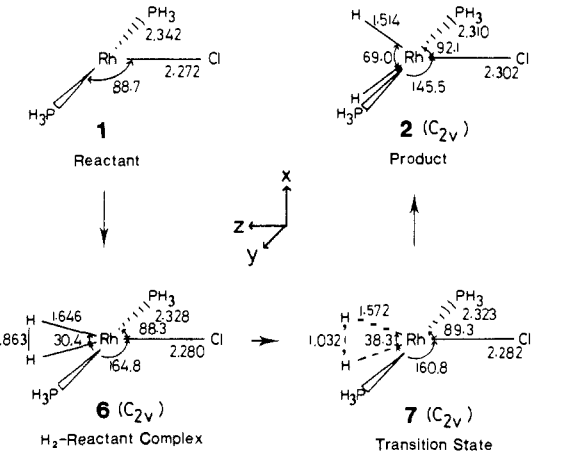


**Figure 1.** Important geometrical parameters of fully optimized geometries (Å and deg) of $RhC(PH_3)_2$ (**1**), the $H_2$–reactant complex **6**, the transition state **7**, and the product $H_2RhCl(PH_3)_2$ (**2**).

five-coordinate intermediate with coplanar ligands. The optimization starting from a T-shaped geometry for the dihydride product (route 2) converged to the $C_{2v}$ Y-shaped geometry **2** of route 1, indicating that the T-shaped intermediate does not exist. A search for a T-shaped transition state also resulted in the Y-shaped ($C_{2v}$) transition state **7**. Therefore we can conclude that the stereochemistry for the addition of $H_2$ to $RhCl(PH_3)_2$ is described by route 1. **6** also converged to a $C_{2v}$ structure.

The optimized structures of the three-coordinate reactant **1**, the weak $H_2$–reactant complex **6**, the transition state **7**, and the dihydride product **2** are shown in Figure 1. The relative energies at the Hartree–Fock level are shown in Table I. The process **1** → **2** is exothermic by 26.4 kcal/mol and an activation barrier from the $H_2$–reactant complex to the dihydride product is 0.6 kcal/mol. These values are to be taken only qualitatively at this level of approximation, since a more refined calculation with a larger basis set and electron correlation would surely change the detailed energetics and could modify the energy profile of the reaction, eliminating this low barrier. Though we have not carried out such a calculation, the present results indicate that the oxidative addition of $H_2$ to this three-coordinate complex takes place very easily, in agreement with the experimental findings.[3b,7b]

In the reactant complex, **6**, the Rh–H bond lengths are only 0.13 Å longer than those of **2**, while the H–H distance (0.863 Å) is substantially longer than that of the molecular hydrogen (0.735 Å). This shows the existence of a strong three-center interaction between $H_2$ and the Rh metal. Interestingly, the optimized structure of **6** is similar to the experimentally determined structure of the molecular hydrogen complex, $W(CO)_3(PR_3)_2(H_2)$, in which the H–H distance is 0.75 Å (X-ray) and 0.82 Å (neutron) and the W–H distance is 1.95 Å (X-ray) and 1.89 Å (neutron).[29] Hay has calculated that the intramolecular oxidative addition from the tungsten $H_2$ complex is endothermic by 17 kcal/mol[30] and has ascribed the stability of this complex to the lowering of the d orbital energy by the $\pi$-acceptor CO ligands. This lowering prevents $\pi$ back-donation from the occupied d orbitals to $H_2$ $\sigma^*$, which would promote the dissociation of $H_2$ to dihydride. In addition, the product is 7-coordinate and thus not stable. The present Rh complex, on the other hand, has no such strong acceptor ligand and the product is 5-coordinate. Therefore, the oxidative addition should take place easily. In the structure of the transition state for the oxidative addition, Rh–H bonds are short, only 0.06 Å longer than those of **2**, indicating that this bond formation is nearly complete. The optimized trigonal-bipyramidal structure of **2** will be discussed again in Section IX.

Figure 2 shows the correlation of important molecular orbitals, obtained in the HF calculation, for the reactants, the $H_2$ complex **6**, and the transition state **7**. This figure, reflecting realistic mixing

(20) GAUSSIAN80[20a] and GAUSSIAN82[20b] program implemented with the L. R. Kahn's ECP program. (a) Binkley, J. S.; Whiteside, R. A.; Krishnan, R.; Seeger, R.; DeFrees, D. J.; Schlegel, H. B.; Topiol, S.; Kahn, L. R.; Pople, J. A. *QCPE* **1981**, *11*, 406. (b) Binkley, J. S.; Frisch, M. J.; DeFrees, D. J.; Raghavachari, K.; Whiteside, R. A.; Schlegel, H. B.; Pople, J. A., Carnegie-Mellon Chemistry Publishing Unit, Pittsburgh, 1984.

(21) Hay, P. J.; Wadt, R. W. *J. Chem. Phys.* **1985**, *82*, 270.

(22) Binkley, J. S.; Pople, J. A.; Hehre, W. J. *J. Am. Chem. Soc.* **1980**, *102*, 939.

(23) Hehre, W. J.; Stewart, R. F.; Pople, J. A. *J. Chem. Phys.* **1969**, *51*, 2657.

(24) Ditchfield, R.; Hehre, W. J.; Pople, J. A. *J. Chem. Phys.* **1971**, *54*, 724.

(25) Huzinaga, S.; Andzelm, J.; Kłobukowski, M.; Radzio-Andzelm, E.; Sakai, Y.; Tatewaki, H. *Gaussian Basis Sets for Molecular Calculations*; Elsevier: Amsterdam, 1984.

(26) Dunning, T. H., Jr. *J. Chem. Phys.* **1970**, *53*, 2823.

(27) (a) Collman, J. P. *Acc. Chem. Res.* **1968**, *1*, 136. (b) Vaska, L. *Acc. Chem. Res.* **1968**, *1*, 335. (c) Halpern, J. *Acc. Chem. Res.* **1970**, *3*, 386.

(28) (a) Yoshida, T.; Otsuka, S. *J. Am. Chem. Soc.* **1977**, *99*, 2134. (b) Yoshida, T.; Yamagata, T.; Tulip, T. H.; Ibers, J. A.; Otsuka, S. *J. Am. Chem. Soc.* **1978**, *100*, 2063.

(29) Kubas, G. J.; Ryan, R. R.; Swanson, B. I.; Vergamini, P. J.; Wasserman, H. J. *J. Am. Chem. Soc.* **1984**, *106*, 451.

(30) Hay, P. J. *J. Am. Chem. Soc.* **1987**, *109*, 705.

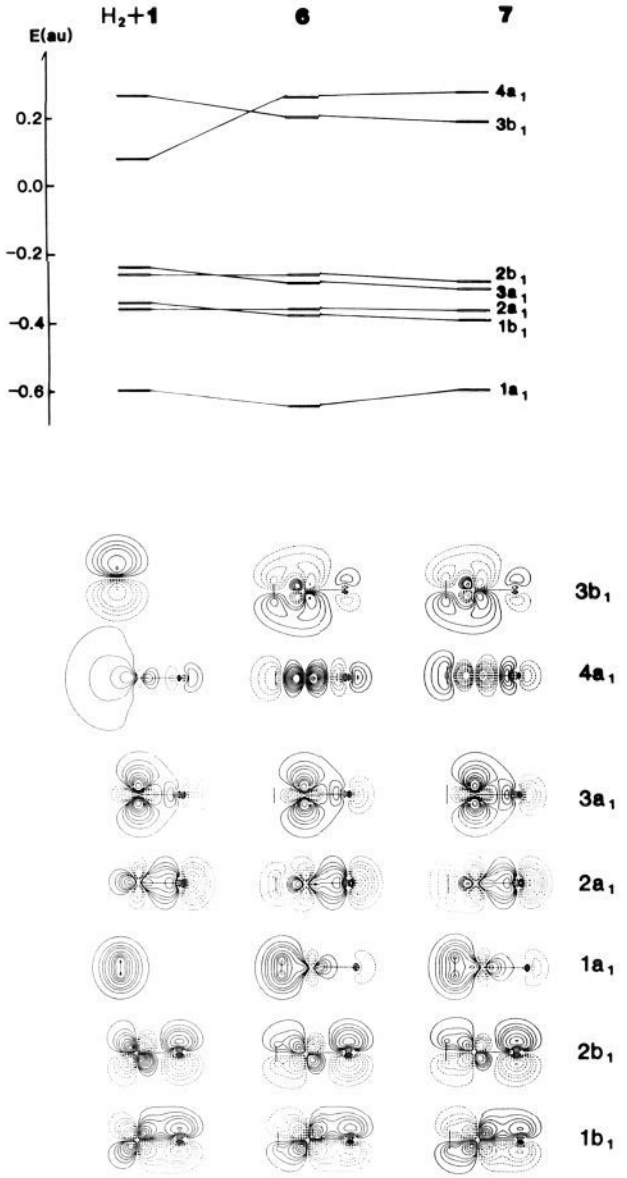


**Figure 2.** Orbital correlation diagram between $H_2$ + $RhCl(PH_3)_2$ and $H_2RhCl(PH_3)_2$.

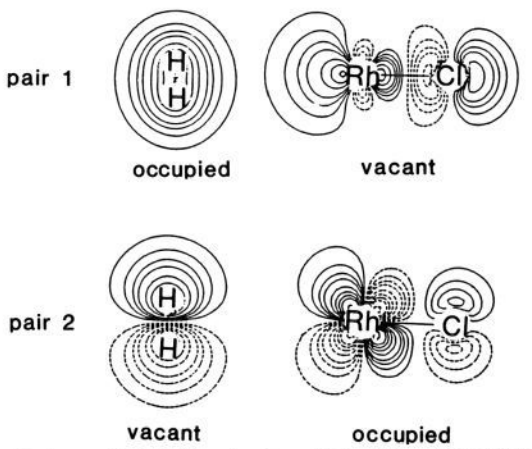


**Figure 3.** Interactive hybrid molecular orbitals of $H_2$ and $RhCl(PH_3)_2$. To avoid overcrowding of contours, the horizontal separation between the two molecules in the figure is taken to be larger than the real distance.

of many molecular orbitals, is not necessarily self-evident. More instructive under such a situation are the interacting hybrid orbitals,[31] two pairs of orbitals of the interacting fragments, obtained by a canonical transformation of the fragment HF orbitals, as shown in Figure 3. One pair of these are the most important occupied MO of the metal fragment $RhCl(PH_3)_2$ and the most important unoccupied orbital of $H_2$, representing the back-donative interaction. The other pair similarly represents the donative interaction from $H_2$ to the metal fragment. The formation of the dihydride is the cooperative result of back-donative interaction from the occupied metal $d_{xz}$ orbital to the $H_2$ $\sigma^*$ orbital and donative interaction from the $H_2$ $\sigma$ orbital into the vacant metal $d_{z^2-y^2}$ orbital. Detailed discussions will be given in Section IX both on the shape of the complex (Y-shaped versus T-shaped) and the energetic contribution of donative and back-donative interactions.

**Scheme III**

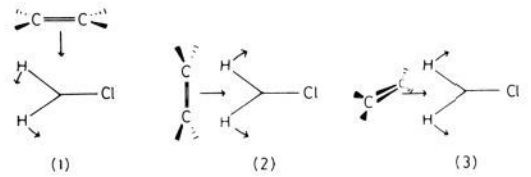


**Scheme IV**

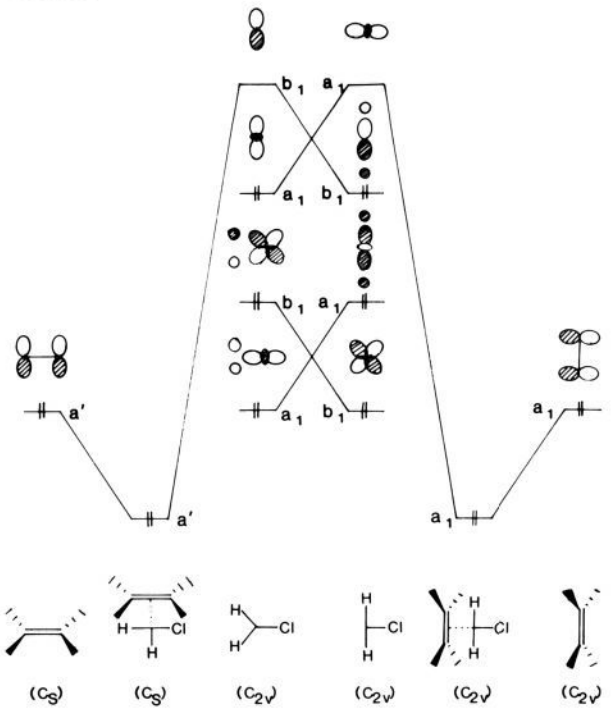


## IV. Olefin Coordination: $H_2RhCl(PH_3)_2 + C_2H_4 \rightarrow H_2RhCl(PH_3)_2(C_2H_4)$

The coordination of olefin to the Y-shaped dihydride $H_2RhCl(PH_3)_2$ (**2**) can proceed in three possible ways, as depicted in Scheme III, even though the second (route 2) and third (route 3) possibilities appear to be unfavored both on steric grounds and in terms of electronic interactions. A look at the qualitative correlation diagram (Scheme IV) shows that the attack of the olefin between the two hydrides giving the trans complex (route 2) is symmetry forbidden,[32] since this process needs the opening of the HRhH angle which is accompanied by an electron transfer from a symmetric ($a_1$) occupied d metal orbital to the antisymmetric ($b_1$) $p_x$ empty orbital. In route 3, the situation of forbidden orbital interaction is similar but the steric repulsion between phosphine ligands and $C_2H_4$ is worse than in route 2. It has been

(31) (a) Fujimoto, H.; Koga, N.; Fukui, K. *J. Am. Chem. Soc.* **1981**, *103*, 7452. (b) Fujimoto, H.; Yamasaki, T.; Mizutani, H.; Koga, N. *J. Am. Chem. Soc.* **1985**, *107*, 6157.

(32) Pearson, R. G. *Acc. Chem. Res.* **1971**, *4*, 152.

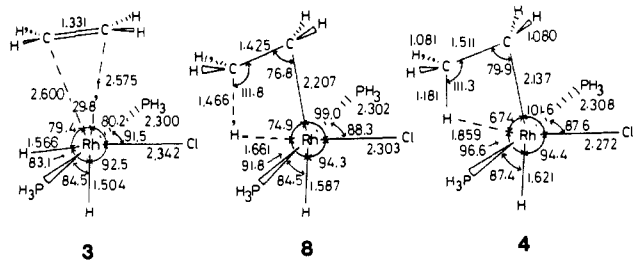


**Figure 4.** Important geometrical parameters of optimized structures (Å and deg) of $H_2RhCl(PH_3)_2(C_2H_4)$ (**3**), $HRhCl(PH_3)_2(C_2H_5)$ (**4**), and the transition state **8** between them.

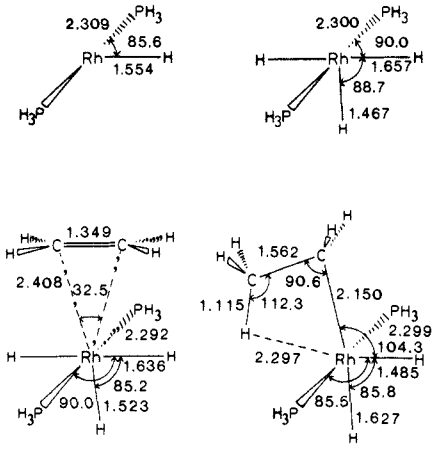

**Figure 5.** Important geometrical parameters of optimized geometries (Å and deg) of $HRh(PH_3)_2$, $H_3Rh(PH_3)_2$, $H_3Rh(PH_3)_2(C_2H_4)$, and $H_2Rh(PH_3)_2(C_2H_5)$.

also suggested both experimentally[3c] and theoretically[10] that the cis dihydride olefin complex, which is formed via route 1 and where the olefin is trans to a hydride, is probably more stable.

Therefore, in our ab initio calculations we have only considered the formation of the cis olefin complex **3**. The optimized geometry of **3** is shown in Figure 4. An extensive search for a transition state connecting the reactants, **2** + $C_2H_4$, and the product **3** has failed, indicating that the olefin coordination reaction takes place without a barrier. The stabilization energy due to coordination has been calculated to be 8.4 kcal/mol at this HF level, a substantial underestimate due to the lack of correlation energy consideration.

One can find in Figure 4 very long Rh–C bonds of 2.60 and 2.58 Å in **3**, though the electron correlation effect might make these distances somewhat shorter. This is not an artifact of calculation; the Rh–C bond length in square-planar $RhCl(PH_3)_2(C_2H_4)$, in which ethylene is trans to chloride, is calculated with the same basis set to be 2.106 Å, in good agreement with the experimental value of 2.122 Å in $RhCl(PPh_3)_2(C_2H_4)$.[33] This suggests that these long Rh–ethylene distances in **3** are due to the strong trans influence of the hydride that is trans to ethylene. In fact the M–C bond lengths calculated in similar Ni– and Pd–ethylene cis dihydride complexes $H_2M(PH_3)(C_2H_4)$ are 2.50 and 2.54 Å for M = Ni and 2.49 and 2.50 Å for M = Pd.[13] The Rh–C distance in $HRh(PH_3)_2(C_2H_4)$ is calculated to be 2.408 Å. In comparison with these distances, the Rh–C distances in **3** are still longer and suggest that there is some effect of cis ligands as well. In order to examine the cis effect, we have optimized the structure of $H_3Rh(PH_3)_2(C_2H_4)$ and it is shown in Figure 5. The two Rh–C distances in Figure 5, both 2.41 Å, are shorter than those in **3** (Figure 4) by 0.2 Å, indicating the existence of a large cis effect difference between hydride and chloride. A cis chloride makes the metal–ethylene bond distance longer than a cis hydride. This trend is opposite to the trend found for the trans effect.

(33) Busetto, C.; D'Alfonso, A.; Maspero, F.; Perego, G.; Zazzetta, A. *J. Chem. Soc., Dalton Trans.* **1977**, 1828.

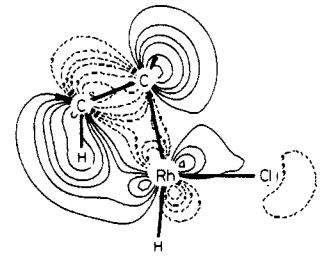

**Figure 6.** Contour map of an occupied MO (19a′) of **4**. The contours are ±0.025, ±0.05, ±0.005, ±0.10, ±0.15, ±0.20, and ±0.25 au, and solid and dotted lines denote positive and negative values, respectively.

This cis effect may be understood by taking into account the $\pi$ back-donating ability of chloride. The key interaction in an ethylene complex is the donative interaction from the $\pi$ orbital of ethylene to a metal vacant orbital consisting mainly of $d_{z^2}$, $p_z$, and s orbital, where the $z$ axis points from the metal to the CC midpoint of ethylene. The competing $\pi$ donative interaction from the Cl $p_z$ orbital reduces the $p_z$ character and hence the directionality of the metal hybrid orbital, making the olefin → metal interaction less effective and therefore the M–C bond weaker. This interference would be small for the $\sigma$-donative hydride. The *cis*-Cl effect as well as the *trans*-H effect will be discussed again in Section IX.

## V. Intramolecular Migratory Olefin Insertion Reaction; $H_2RhCl(PH_3)_2(C_2H_4) \rightarrow HRhCl(PH_3)_2(C_2H_5)$

As was discussed in the Introduction, this intramolecular migratory olefin insertion step has been established to be the rate-determining step in the mechanism proposed by Halpern et al.[3] Despite the importance of olefin hydrides in catalytic cycles, such species have rarely been amenable to mechanistic investigation. The equilibrium between a transition-metal olefin hydride and the corresponding alkyl species has been observed only rarely,[34] due to the kinetic instability of transition-metal alkyls. Although alkyl hydride intermediates have often been postulated in a homogeneous catalytic hydrogenation, very few have been experimentally observed.[35]

One interesting question concerning this reaction has been whether the formation of ethyl complex takes place via olefin insertion into the M–H bond or via hydride migration to the coordinated olefin. In a theoretical study Dedieu[10] has suggested that in the early stage of reaction olefin moves toward the hydride group. Koga et al. have actually determined the transition state for olefin insertion/$\beta$-elimination of Ni, Pd, and Pt complexes, $HM(PH_3)(C_2H_5) \rightleftarrows H_2M(PH_3)(C_2H_4)$, to find that the reaction takes place only via hydride migration.[13]

In Figure 4 we show the optimized geometries for the olefin dihydride complex **3** (the reactant), the *trans*-ethyl complex **4** (the product), and the transition state **8** connecting **3** and **4**.

The structural changes during the reaction are such that the symmetrically $\eta^2$-coordinated olefin at first shifts its position to the left in Figure 4 to give an $\eta^1$-coordination and then picks up the hydride from the metal at its uncoordinated carbon. The reaction is thus described as a hydrogen migration, as was the case for similar reactions of Ni, Pd, and Pt complexes.[13] At the transition state **8**, the CRhCl angle and the RhCC angle are close to those of the product; the stage of the position shift of ethylene is nearly complete. The succeeding hydride migration stage is in progress; for instance, the CC bond distance in **8** is nearly at the midpoint between that of the reactant and the product. The transition state is a relatively "late" transition state in the overall intramolecular hydrogen migratory insertion reaction. This is in contrast with the intramolecular hydrogen migratory insertion of

(34) (a) Werner, H.; Feser, R. *Angew. Chem., Int. Ed. Engl.* **1979**, *18*, 157. (b) Werner, H.; Feser, R. *J. Organomet. Chem.* **1982**, *232*, 351. (c) Chaudret, B. N.; Cole-Hamilton, D. J.; Wilkinson, G. *Acta. Chem. Scand., Ser. A* **1978**, *A32*, 763. (d) Seiwell, L. P. *Inorg. Chem.* **1976**, *15*, 2560. (e) Klein, H. F.; Hammer, R.; Gross, J.; Schubert, U. *Angew. Chem., Int. Ed. Engl.* **1980**, *19*, 809.

(35) Chan, A. S. C.; Halpern, J. *J. Am. Chem. Soc.* **1980**, *102*, 838.

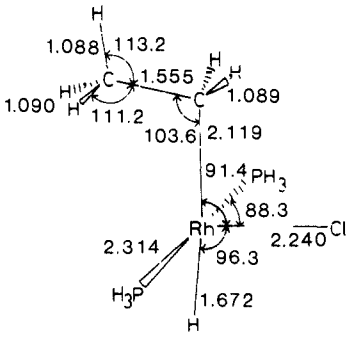


**Figure 7.** Important geometrical parameters of the fully optimized geometry (Å and deg) of staggered $HRhCl(PH_3)_2(C_2H_5)$ (**4A**).

similar Ni and Pd complexes, where the transition state was found to be relatively "early".[13] This point will be discussed in detail in Section IX.

The ethyl complex **4** has a distorted ethyl group with the small Rh–C–C angle of about 80°, a short Rh···H distance, and the long C–H$^\beta$ bond of 1.18 Å (compared to normal 1.08 Å) indicating the existence of a very strong agostic interaction.[36] As shown in Figure 6 a strong donative interaction from the CH bond to a vacant Rh d orbital takes place in the ethyl complex and is the origin of the agostic interaction.[17] The distortion in **4** is larger than those we previously found in Ti and Pd complexes.[13,17]

However, the optimized structure of $H_2Rh(PH_3)_2(C_2H_5)$ shown in Figure 5, in which Cl of **4** is replaced by H, has a smaller distorted structure similar to the Ti and Pd complexes. This indicates that the large distortion is ascribed to the electronic effect of chloride. The $\sigma$ electron-withdrawing chlorine ligand trans to the vacant coordination site makes the electron donation from the CH bond to the vacant Rh d orbital easier and the agostic interaction stronger. In addition, $\pi$ electron donation of the chloride makes the Rh–ethyl bond weaker, a situation similar to the Rh–ethylene bond as discussed in the preceding section, leading to the larger distortion.

The optimization of complex **4A** with the staggered conformation gave a different result as shown in Figure 7. The RhCC angle of 104° is larger by 24° than that of **4** and the CH$^\beta$ bond lengths are normal, indicating weak or no agostic interaction. In **4A** the overlap and therefore the donative interaction between the CH$^\beta$ $\sigma$ orbital and the unoccupied d orbital is smaller. **4A** is 3.5 kcal/mol higher than **4**. If we assume 2.9 kcal/mol as the rotation barrier of the ethyl group, the agostic interaction energy can be estimated to be 6.4 kcal/mol, larger than that of the Pd complex, 3.3 kcal/mol, consistent with the larger distortion of the ethyl group.

Since this is the most important step of the catalytic cycle, we have carried out better energy calculations, with the larger basis set II and with the electron correlation at the MP2 level, at the geometries optimized with the basis set I at the HF level. The results are shown in Table II. Table II shows at first that, regardless of the basis set and the electron correlation, the reaction is quite endothermic. Considering together the results in the preceding section that the combined $H_2$ oxidative addition + olefin coordination step is very exothermic, the ethylene complex **3** seems to be an intermediate with a finite lifetime and may be detectable experimentally.

The use of the larger basis set increases the energy of the ethyl complex **4** relative to the ethylene complex **3**. This energy increases further with the inclusion of the correlation energy.[37] With use of the geometries optimized at the HF level with the smaller basis set I, the larger basis set or the electron correlation makes the energy of the product **4** higher than that of the transition state **8**. At the present level of calculation, all one can say would be that the potential energy profile for the intramolecular migratory olefin insertion reaction is uphill from the reactant to the product with a small or no hump.

**Table II.** Calculated Relative Energies (kcal/mol) for the Reaction $H_2RhCl(PH_3)_2(C_2H_4) \rightarrow HRhCl(PH_3)_2(C_2H_5)$

| basis | method | $H_2RhCl(PH_3)_2(C_2H_4)$ (**3**) | transition state **8** | $HRhCl(PH_3)_2(C_2H_5)$ (**4**) |
|---|---|---|---|---|
| I[a] | RHF | −1201.99269[c] | +18.4 | +16.4 |
| | MP2 | −1202.45388[c] | +17.1 | +21.0 |
| II[b] | RHF | −1244.26877[c] | +22.1 | +23.7 |
| | MP2 | −1244.82751[c] | +18.6 | +25.5 |

[a] With the smaller basis set I. [b] With the larger basis set II. [c] The total energy in hartrees and the reference for the relative energy.

The range of calculated endothermicity/activation energy is not far from the experimental activation energies for the hydrogenation of cyclohexene in benzene, 7 to 19 kcal/mol.[2,38] There is also an experimental result that the alkyl hydride intermediate formation is a reversible reaction for trisubstituted cyclohexene[39] but could be considered irreversible near room temperature in the case of less highly substituted alkene.[40,41]

The high instability of the ethyl complex **4** is attributable to the strong trans influence of the hydride as well as to the strong cis influence of the chloride, as was discussed above and will be discussed in detail in Section IX.

## VI. Isomerization of $HRhCl(PH_3)_2(C_2H_5)$

The ethyl complex **4**, formed by $H_2$ oxidative addition and subsequent olefin coordination and insertion, has the ethyl group trans to the hydride. In order for the reductive elimination of ethane to take place, these two groups have to be cis to each other. Though the isomerization process is not explicitly included in the Halpern mechanism (Scheme I) of the catalytic cycle, it is an important step that has to be examined carefully.

We have investigated possible isomerization paths from the *trans*-ethyl **4** to several cis isomers and conformations. The elementary steps which could constitute the overall isomerization are the hydride migration, as well as the chloride migration, the ethyl group migration, the ethyl group rotation around the Rh–C bond, and the eclipsed → staggered internal rotation around the ethyl C–C bond. These steps might take place in various orders in sequence or some in parallel.

In order to compare the relative stability of the various cis isomers and conformations, we have at first determined the fully optimized geometries of six cis isomers/conformations under the assumption of $C_s$ symmetry, four of them (**5B**, **5B′**, **5C**, **5C′**) having a vacant site trans to the hydride and two (**5A** and **5A′**) trans to the ethyl group. The optimized structures are shown in Figure 8 and energies relative to **4** in Figure 9. The geometry optimization for **5D** converged to **5C**, indicating that **5D** is not a stationary point on the potential energy surface. All the conformations with the ethyl group in the eclipsed conformation (**5A′**, **5B′**, and **5C′**) are found to be a transition state for the ethyl CC internal rotation, connecting the corresponding staggered conformations, which are equilibrium geometries (**5A**, **5B**, and **5C**). The reductive elimination of ethane can thus take place from either **5A**, **5B**, or **5C**. All the stable ethyl complexes are found to have a T-shaped structure, with the vacant site located on one principal axis of the $O_h$ skeleton.

(36) Brookhart, M.; Green, M. L. H. *J. Organomet. Chem.* **1983**, *250*, 395.
(37) A similar trend has been found in other cases. For instance the insertion of CO in $HMn(CO)_5$, calculated to be endothermic by 10.5 kcal/mol with an activation energy of 14.4 kcal/mol at the HF level, increases the endothermicity to 38.4 kcal/mol and a barrier to 38.8 kcal/mol with the CI calculation. A similar trend is followed on going from HF to MP2 for the hydride migration in HMnCO or the methyl migration in $CH_3MnCO$.[37a] (a) Dedieu, A. *Quantum Chemistry: The Challenge of Transition Metals and Coordination Chemistry*; Veillard, A. Ed.; Reidel: Dordrecht, 1986; NATO ASI Series C, Vol. 176. (b) Dedieu, A.; Sakaki, S.; Strich, A.; Siegbahn, P. E. M. *Chem. Phys. Lett.* **1987**, *133*, 317.
(38) McGrady, N. D.; McDade, C.; Bercaw, J. E. *Organometallic Compounds: Synthesis, Structure and Theory, Proceedings of the Symposium of the Industry–University Cooperative Chemistry Program*; Shapiro, B. L. Ed.; Texas A&M University Press: College Station TX, 1983; pp 46–85.
(39) Demortier, Y.; de Aguirre, I. *Bull. Soc. Chim. Fr.* **1974**, 1614, 1619.
(40) (a) Hussey, A. S.; Takeuchi, Y. *J. Am. Chem. Soc.* **1969**, *91*, 672. (b) Hussey, A. S.; Takeuchi, Y. *J. Org. Chem.* **1970**, *35*, 643.
(41) Biellmann, J. F.; Jung, M. J. *J. Am. Chem. Soc.* **1968**, *90*, 1673.

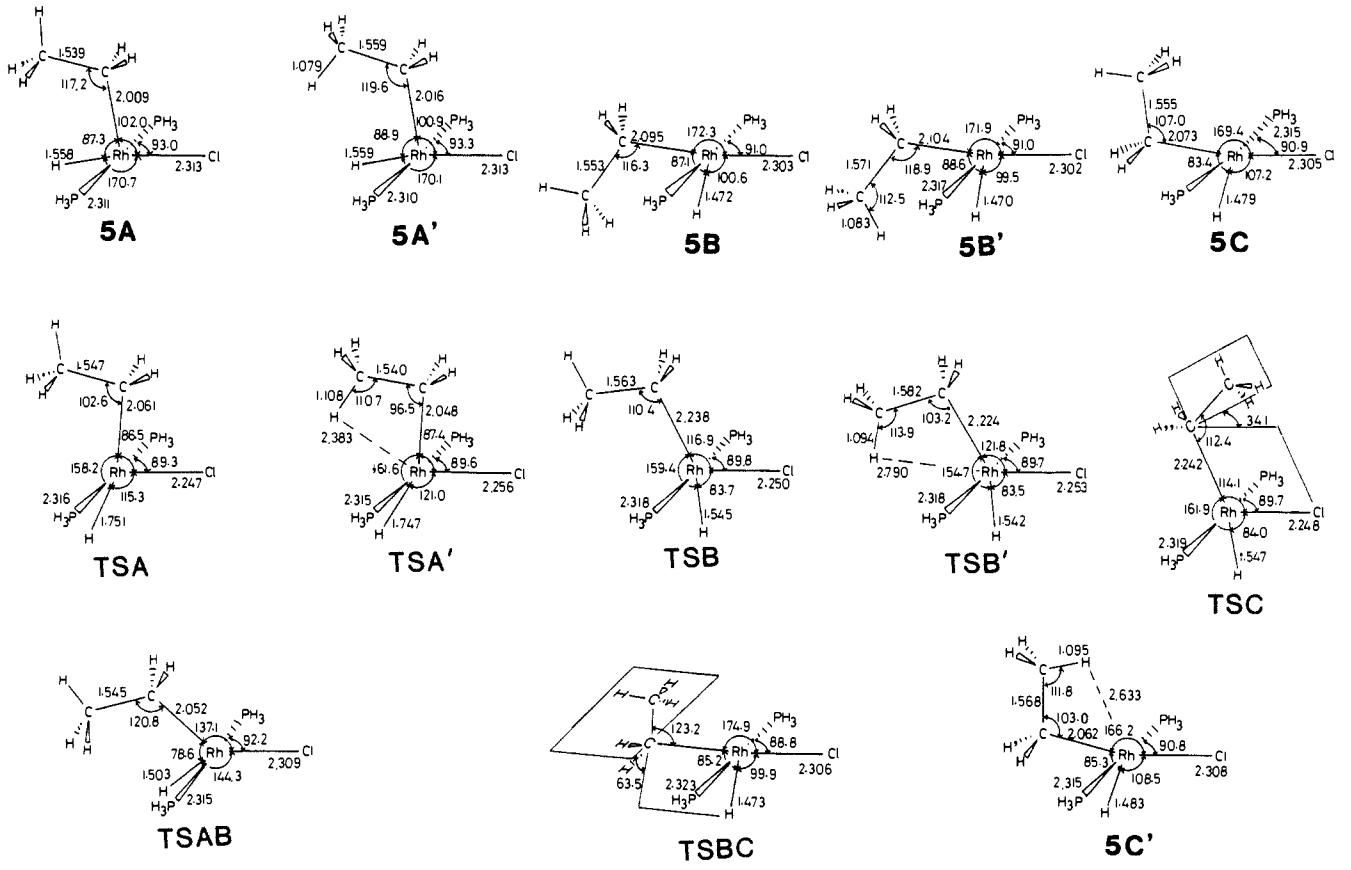


**Figure 8.** Important geometrical parameters of optimized structures (Å and deg) of isomers and conformers of $HRhCl(PH_3)_2(C_2H_5)$ and some transition states involved in the isomerization process.

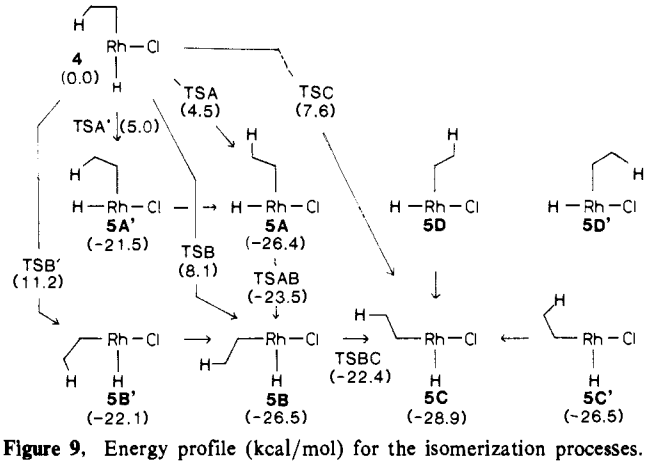


**Figure 9.** Energy profile (kcal/mol) for the isomerization processes.

In passing we will make a few comments on the structure of **5C'**, which does not show an agostic interaction, in contrast to the agostic structure of **4**. The only difference between **4** and **5C'** is the position of the hydride and the chloride ligands. As was discussed in Section V, both the hydride trans to ethyl and the chloride cis to ethyl are responsible to the agostic interaction. In **5C'**, the positions of both ligands are switched; the cis hydride and the trans chloride are not capable of causing an agostic interaction.

The most stable isomer is **5C**, lower in energy than **4** by 29 kcal/mol, in which the open coordination site is located trans to the strong trans-influencing hydride and the HRhCC is in the least crowded trans conformation. The isomers **5B** and **5A**, with the HRhCC in the more crowded cis conformation, are higher in energy than **5C** by about 2 kcal/mol.

One notices that all the isomers, **5**'s, where the hydride and the ethyl are cis to each other, are over 20 kcal/mol more stable than the trans isomer **4**. This is due to the trans influence of the hydride as well as the cis influence of the chloride to the stability of the alkyl–metal bond. A comparison of energies between **5A** and **5B** and between **5D** and **5C** suggests that the influence between hydride and chloride is slightly larger than that between alkyl and chloride.

The transition states connecting **4** to **5A**, **5A'**, **5B**, **5B'**, and **5C**, determined under the $C_s$ symmetry constraint as TSA, TSA', TSB, TSB', and TSC, respectively, are shown in Figure 8 for geometries and in Figure 9 for relative energies. The transition states connecting **5A** to **5B** and **5B** to **5C** are also determined as TSAB and TSBC, respectively. In determining TSC and TSBC, which involve the rotation of the ethyl group around the RhC bond, the local $C_s$ symmetry of the Rh–ethyl fragment has been assumed, and therefore, their energies should be taken as upper limits, though no large change is expected to occur upon relaxation of the constraint. Some of the TS's determined above may not be real transition states. For instance, TSA' probably has two imaginary frequencies, one along the hydride migration coordinate and another for the internal rotation around the ethyl CC bond, which will lead to the true transition state TSA about 0.5 kcal/mol lower in energy at this level of calculation. (See below for the correlation effect.)

One notices all the transition states of hydride, chloride, or alkyl migration, or of a combination of migration and internal rotation, i.e., all TS's in Figure 8 except for TSBC have a trigonal-bipyramidal, Y-shaped structure, a structure situated between the two T-shaped structures of the reactant and the product.

Starting from the equilibrium structure **4** of the trans hydride ethyl complex, one can reach a cis complex **5A** directly by a simultaneous hydride migration and ethyl CC internal rotation TSA, with a small activation energy of 4.5 kcal/mol. The sequential isomerization first to **5A'** via hydride migration and then to **5A** via ethyl internal rotation requires a slightly larger activation energy at this level of calculation. There are three routes going from **4** to another cis complex **5B**. The best is the hydride migration to **5A**, mentioned above, followed by the chloride migration with a small barrier of about 3 kcal/mol. The simultaneous ethyl migration/ethyl internal rotation through TSB requires an ac-

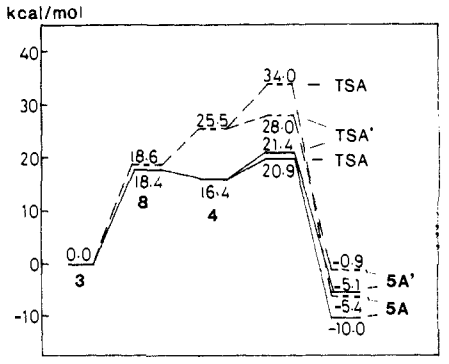


**Figure 10.** HF (—) and MP2 (---) energy profiles for the rate-determining step.

**Table III.** Relative Energy (kcal/mol) for the Two Lowest Initial Isomerization Paths: *trans*-Ethyl Intermediate **4** → *cis*-**5A** and **5A'**

| basis | method | 4 | TSA' | 5A' | TSA | 5A |
|---|---|---|---|---|---|---|
| I[a] | HF | 0 | +5.0 | -21.5 | +4.5 | -26.4 |
| II[b] | HF | 0 | +4.4 | -25.7 | +6.6 | -30.1 |
| | MP2 | 0 | +2.5 | -26.4 | +8.5 | -30.8 |

[a] With the smaller basis set I. [b] With the larger basis set II, at the geometries optimized at the HF/basis I level.

tivation energy of about 8 kcal/mol. The other is the alkyl migration from **4** to **5B'**, with a barrier of about 11 kcal/mol, and **5B'** goes to **5B** without barrier. The above energetics shows that the sequential migration of hydride and chloride takes place more easily than the single migration of the alkyl group. Since the Rh–C bond is weaker than the Rh–H bond, as will be discussed later, the difficulty of the alkyl migration must be related to the directionality of the alkyl $\sigma$ orbital.[12c] The hydride, which uses a spherical 1s orbital for bonding, would be able to interact more easily with two orbitals, while the alkyl with a directed $sp^3$ hybrid orbital would have difficulty in simultaneously attractively interacting with two metal orbitals during migration.

Another cis complex **5C** is reachable via various routes. The best is a sequential route **4** –(hydride migration→ **5A** –(chloride migration)→ **5B** –(rotation of ethyl group around the RhC axis)→ **5C**. Whatever route one may take, one has to rotate the ethyl group around the RhC axis to reach **5C** from **4**. This rotation is sterically impossible if any bulky group is on the phosphine. In the actual catalytic system, $PPh_3$ is used. Therefore it is not likely that the intermediate **5C** is important in the catalytic process.

Though the barrier for isomerization of **4** is only a few to several kcal/mol, it plays an important role in the rate-determining step. As shown in Figure 10, the trans hydride complex **4** is in a shallow energy minimum at the HF level (or a transient species with no stability at the MP2 level), after climbing up the rate-determining barrier for olefin insertion. A small barrier for isomerization adds up to this rate-determining barrier, making the effective barrier higher. One should rather say that the rate-determining step is the combination of the olefin migratory insertion and the isomerization.

In order to assess the effect of the electron correlation to the rate-determining barrier, we have carried out energy calculations for TSA, TSA', **5A**, and **5A'** at the MP2 level with the larger basis set II at the optimized geometries at the HF/basis I level. The results are shown in Table III and Figure 10. With the electron correlation, the sequential isomerization to **5A** through TSA' and **5A'** becomes substantially more favorable than the direct route through TSA. Probably the actual reaction route involves the ethyl CC internal rotation immediately after the transition state TSA' to reach **5A** without actually passing through **5A'**. At this level of calculation, the potential energy profile is uphill all the way from the olefin complex **3** to the transition state for isomerization TSA'.

### VII. Reductive Elimination of Ethane: $HRhCl(PH_3)_2(C_2H_5) \rightarrow RhCl(PH_3)_2 + C_2H_6$

The reductive elimination process is well documented both experimentally[42] and theoretically,[12,43] since this reaction is involved

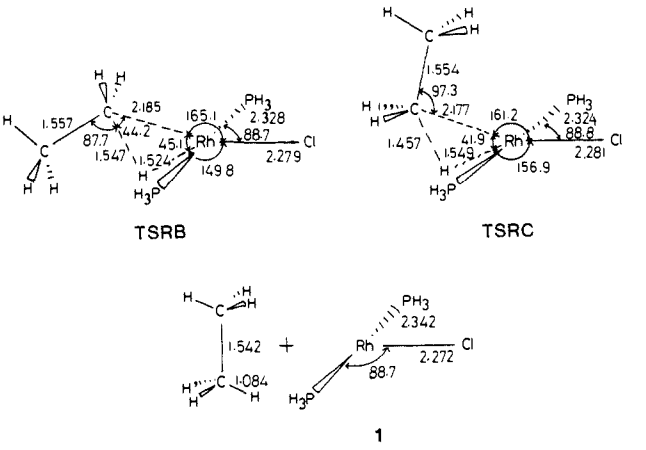


**Figure 11.** Important geometrical parameters of optimized structures (Å and deg) of the transition states and products of the reductive elimination $HRhCl(PH_3)_2(C_2H_5) \rightarrow RhCl(PH_3)_2 + C_2H_6$.

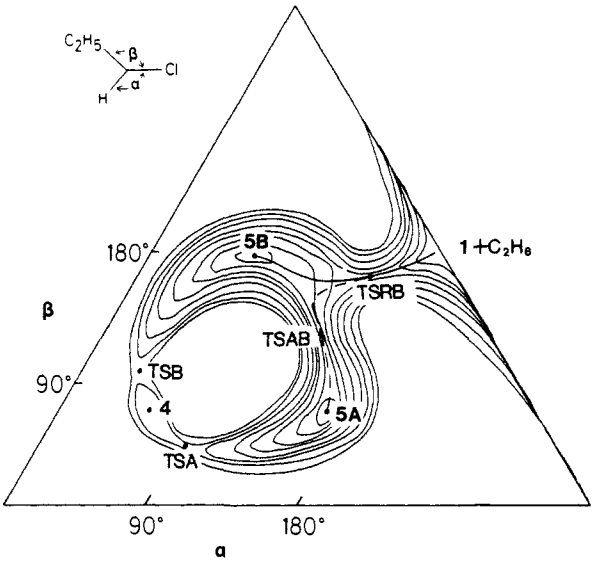


**Figure 12.** The qualitative potential energy surface of $HRhCl(PH_3)_2(C_2H_5)$ as a function of $\alpha$ and $\beta$. Contours are for every 5 kcal/mol.

in many catalytic cycles. Recently thorough ab initio MO theoretical studies of the reductive elimination of $CH_4$ from $HPt(CH_3)(PH_3)_2$ have been carried out.[12]

As was discussed in the Introduction, the reductive elimination of ethane from $HRhCl(PH_3)_2(C_2H_5)$ in the Wilkinson catalytic cycle is considered to be fast. Any of the three isomers **5A**, **5B**, or **5C** of the *cis*-ethyl complex in Figure 9 may be actively involved in the reductive elimination. We have found two transition states for this process, TSRB and TSRC, shown in Figure 11. Both are again Y-shaped, as was the case of other 5-coordinate transition states. TSRC has the HRhCC skeleton in the trans conformation, while TSRB has it in the cis conformation. Since **5D** does not exist, TSRC is considered to be the transition state from **5C**. On the other hand, TSRB has a geometry somewhere between that of **5A** and **5B** and cannot be easily assigned to the transition

(42) (a) Milstein, D.; Stille, J. K. *J. Am. Chem. Soc.* **1979**, *101*, 4981. (b) Gillie, A.; Stille, J. K. *Ibid.* **1980**, *102*, 4933. (c) Tamaki, A.; Magennis, S. A.; Kochi, J. K. *J. Am. Chem. Soc.* **1974**, *96*, 6140. (d) Tamaki, A.; Kochi, J. K. *J. Organomet. Chem.* **1972**, *40*, C81; **1973**, *51*, C39. (e) Whitesides, G. M.; Gaasch, J. F.; Stedronsky, E. R. *J. Am. Chem. Soc.* **1972**, *94*, 5258. (f) Young, G. B.; Whitesides, G. M. *Ibid.* **1978**, *100*, 5808. (g) Brown, M. P.; Puddephatt, R. J.; Upton, C. E. E. *J. Organomet. Chem.* **1973**, *49*, C61; *J. Chem. Soc., Dalton Trans.* **1974**, 2457. (h) Ozawa, F.; Ito, T.; Nakamura, Y.; Yamamoto, A. *Bull. Chem. Soc. Jpn.* **1981**, *54*, 1868.

(43) (a) Komiya, S.; Albright, T. A.; Hoffmann, R.; Kochi, J. K. *J. Am. Chem. Soc.* **1976**, *98*, 7255; **1977**, *99*, 8440. (b) Tatsumi, K.; Hoffmann, R.; Yamamoto, A.; Stille, J. K. *Bull. Chem. Soc. Jpn.* **1981**, *54*, 1857. (c) Balazs, A. C.; Johnson, K. H.; Whitesides, G. A. *Inorg. Chem.* **1982**, *21*, 2162.

Table IV. Calculated Relative HF Energy (kcal/mol) for the Reaction $HRhCl(PH_3)_2(C_2H_5) \rightarrow RhCl(PH_3)_2 + C_2H_6$

| cis ethyl complex $HRhCl(PH_3)_2(C_2H_5)$ | transition state | $HRhCl(PH_3)_2$ (1) + $C_2H_6$ |
|---|---|---|
| **5A** +2.5 | | |
| **5B** +2.4 | TSRB +17.7 | +3.4 |
| **5C** 0[a] | TSRC +14.3 | |

[a] The total energy is −1202.01268 hartrees.

state from **5A** or from **5B**. An extensive search also suggests that another transition state does not exist in the vicinity. A steepest descent walk on the potential energy surface from a point near TSRB has clearly indicated that TSRB is the transition state from **5B**, implying that the transition state from **5A** does not exist.

The region of the potential surface in the vicinity of **5A**, **5B**, and TSB has been explored a little more thoroughly. Figure 12 is a schematic representation of the surface as a function of the HRhCl angle $\alpha$ and the CRhCl angle $\beta$. Tracing backward from the reductive elimination product **1** ($\alpha = \beta = 180°$), the reaction path passes through TSB where $\beta$ is slightly larger than $\alpha$ and bends sharply by decreasing $\alpha$ to reach **5B**. There is no direct path open from **5A** to **1**. The reductive elimination from **5A** has to go through a low energy transition state TSAB by migrating Cl (increasing $\alpha$ and decreasing $\beta$ by nearly the same amount). It is probably not necessary to complete the Cl migration and reach **5B**, but rather the trajectory can turn (dotted line in Figure 12) by increasing both $\alpha$ and $\beta$ and climb a barrier to reach TSRB and eventually to the product **1**.

The transition-state geometries in Figure 11 show that the largest change is in the HRhC angle, which is reduced from 87° (**5B**) and 83° (**5C**) to 45° (TSRB) and 42° (TSRC), respectively. The Rh–H and the Rh–C bonds, however, are only about 5% longer in the transition states than in the reactants, and the newly formed C–H bond is much longer than that in ethane. Thus, these transition states are characterized as early. Both the Rh–H and the Rh–C bonds are breaking synchronously.

In Table IV we show the potential energy profile for the reductive elimination at the HF level. The reaction is essentially thermoneutral. The activation barrier is 14.3 kcal/mol from **5C** to TSRC and 15.3 kcal/mol from **5B** to TSRB. As was discussed above, the effective barrier for the reaction of **5A**, i.e., **5A** → TSAB → TSB, is also the same.

As was discussed in Section VI, the complex with bulky phosphines will be hindered from reaching **5C**. Regardless of whether the reductive elimination takes place from **5A** or **5B**, the barrier is substantial. However, this is much lower than the barrier for the combined olefin insertion + isomerization and is not the rate-determining step.

The main bonding interactions between $C_2H_5$ + H and Rh at the transition states are depicted below.

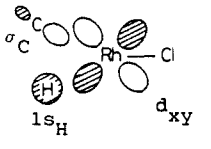


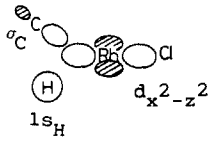


The linear combinations of the ethyl terminal carbon $\sigma$ orbital and the hydrogen 1s orbital, $\sigma_C + 1s_H$ and $\sigma_C - 1s_H$, which lead to the CH $\sigma$ and the CH $\sigma^*$ orbital, respectively, of ethane, overlap with the metal $d_{xz}$ and $d_{z^2-y^2}$, respectively, contributing to the stabilization of the transition state. The transition state is not on the least-motion path, on which the transition state would be T-shaped. The orbital interaction between the CH $\sigma$ orbital and unoccupied $d_{z^2-y^2}$ makes the Y-shaped transition state favorable. If the transition state is T-shaped, a strong exchange repulsion between the occupied CH $\sigma$ orbital and the occupied $d_{xz}$ would take place.

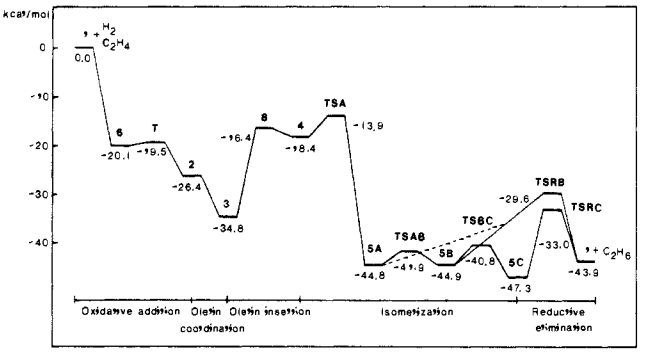


**Figure 13.** The potential energy profile of the entire catalytic cycle (kcal/mol) at the HF level.

In the present study, we have examined two oxidative addition reactions, the $H_2$ addition in Section III and the $C_2H_6$ addition, e.g., the reverse of the reductive elimination in this section. When these two reactions are compared, the metal–carbon and –hydrogen binding energy $D$ can be estimated. The exothermicity of the $H_2$ and $C_2H_6$ oxidative addition reaction can be considered to be equal to $2D(Rh-H) - D(H-H)$ and $D(Rh-H) + D(Rh-C) - D(C_2H_5-H)$, respectively.[44] Using the HF/3-21G value of $D(H-H) = 81.9$ and $D(C_2H_5-H) = 86.3$ kcal/mol, and the exothermicity in Tables I and IV (with the most stable **5C**), one obtains estimates of $D(Rh-C) = 35.5$ and $D(Rh-H) = 54.2$ kcal/mol, respectively. The trend that the M–H bond is stronger than the M-C bond is in agreement with the general trend of many organometallic complexes.[12,14] This difference in the binding energy is why the oxidative addition of $H_2$ is more exothermic than that of $C_2H_6$. This is one of the reasons why the activation barrier of $C_2H_6$ oxidative addition is higher than that of $H_2$ oxidative addition, although the directionality of the ethyl $sp^3$ orbital, compared with the spherical hydrogen 1s orbital, may also make the barrier higher as was proposed by Low and Goddard.[12c]

## VIII. Reaction Mechanism of the Full Catalytic Cycle: Results and Perspective

After examining five steps of elementary reactions, we have regenerated the original catalyst **1** and have come around a full catalytic cycle. In Figure 13, we show the potential energy profile for the full cycle at the HF level. Energetics at the MP2 level for some key steps has been shown in Figure 10. The energy difference between the two ends of the profile corresponds to the energy of reaction $H_2 + CH_2{=}CH_2 \rightarrow CH_3CH_3$. The calculated energy difference at the present HF/3-21G level, 43.9 kcal/mol, may be compared with the experimental standard heat of reaction, 32.7 kcal/mol, obtained from the standard heats of formation.[45] The 6-31G* RHF and MP2 geometry optimization calculations have given 44.0 and 41.1 kcal/mol, respectively.[46]

The potential energy profile in Figure 13 is remarkably smooth. There is no barrier that is too high. There is no intermediate that is too stable to break the chain of reactions. Any good catalytic system, of course, has to satisfy these criteria, and quite certainly the Wilkinson catalyst system does satisfy. This is, however, the first time that this behavior of the potential energy profile has been seen directly in a theoretical calculation.

The first two reactions, oxidative addition of $H_2$ to give $H_2RhCl(PH_3)_2$ and coordination of olefin to give $H_2RhCl(PH_3)_2(C_2H_4)$, are found to be exothermic and proceed with little or no activation barrier. The intramolecular olefin migratory insertion

(44) $D$(Pt–C) and $D$(Pt–H) have been theoretically estimated to be 34 and 70 kcal/mol, respectively, from calculations on the oxidative additions: $Pt(PH_3)_2 + H_2$ and $Pt(PH_3)_2 + CH_4$.[12b]

(45) Wagman, D. D.; Evans, W. H.; Parker, V. B.; Schumm, R. H.; Halow, I.; Bailey, S. M.; Churney, K. L.; Nuttall, R. L. *J. Phys. Chem. Ref. Data, Suppl. 2* **1982**, *11*.

(46) *Carnegie-Mellon Quantum Chemistry Archive*; Whiteside, R. A., Frisch, M. J., Pople, J. A., Eds.; Carnegie-Mellon University: Pittsburgh, 1983.

reaction to give $HRhCl(PH_3)_2(C_2H_5)$, combined with the first step of isomerization of the trans ethyl hydride complex to a cis complex, is exothermic overall and appears to take place as one combined step. This combined step has the highest activation barrier of about 20–25 kcal/mol and is found to be the rate-determining step in the present calculation. This characteristic is consistent with the experiments and Halpern's mechanism,[3] which propose the migratory insertion is the rate-determining step. The present theoretical calculation suggests that the rate-determining step actually includes a part of trans → cis isomerization processes. The overall trans → cis isomerization is highly exothermic and takes place with a small activation energy preferrable via hydride and chloride migration rather than via alkyl migration. The final reductive elimination of ethane to regenerate $RhCl(PH_3)_2$ is nearly thermoneutral and has an activation barrier substantial but smaller than that of the rate-determining step. Therefore, neither isomerization nor H/D scrambling of olefin can take place.

We have been able to obtain the potential energy profile of a full catalytic cycle with the ab initio MO study by determining the structures and the energies of the intermediates and transition states of the constituting elementary reactions. However, many words of caution would be needed at the present stage.

On the theoretical side, the present basis sets are limited and the level of the electron correlation has been minimal. A larger basis set would be needed to avoid the superposition error, in particular, when the coordinating interaction is important as in the olefin coordination step. The correlation would definitely change the quantitative energetics. All the intermediates examined in the present study have at least three strong ligands, two phosphines and a chloride, and hence quite certainly have a closed shell ground state. Therefore, our experiences[12a,b,13,14,16] on several organometallic elementary reactions suggest that the geometries optimized at the HF level would be quite reasonable. However, the HF energetics may not be. Our calculation with a larger basis set and MP2 electron correlation for a few critical steps indicate that the energies change and some transition states disappear. However, the correlation did not change the overall qualitative characteristics of the potential profile.

From the point of view of an experimentalist, our present study will be blamed for several simplifications in the model system. For one we adopted $PH_3$ in place of experimentally used $PPh_3$. We think that the present study with $PH_3$ provides essential and basis information of the catalytic system. Because of its steric and electronic effects, a bulky phosphine will modify parts of the potential surfaces, as we found before in the $Pt(PR_3)_2 + H_2$ oxidative addition reaction.[12b] In the present study we have qualitatively taken into account the steric hindrance of bulky phosphine during the isomerization step. We hope to extend our study in the future to the role of $PPh_3$ in the catalytic cycle.

As to the substrate, our model olefin $C_2H_4$ is well-known not to be catalyzed under the usual condition; the stable $RhCl(PPh_3)_2(C_2H_4)$ stops the catalytic cycle. Our calculation shows that $RhCl(PH_3)_2(C_2H_4)$ is a stable complex, with the $C_2H_4$ binding energy of 35 kcal/mol at the RHF level. The oxidative addition of $H_2$ to $d^8$ four-coordinate $RhCl(PH_3)_2(C_2H_4)$, one of the steps in unsaturated mechanism, is much more difficult. Since the vacant metal orbital which favors the oxidative addition as discussed in Section III does not exist, it would require a higher activation energy. The transition-state search of this $H_2$ oxidative addition resulted in $C_2H_4$ dissociation, whose endothermicity is 35 kcal/mol. The $C_2H_4$ dissociation gives the vacant coordination site and thus a low-lying vacant metal orbital, which will facilitate the $H_2$ oxidative addition. This supports the so-called hydride mechanism, olefin coordination after $H_2$ oxidative addition, for the neutral catalytic system. The present calculation thus suggests that the ethylene hydrogenation would not be impossible if $H_2$ oxidative addition could take place prior to $C_2H_4$ coordination.

The steric hindrance due to bulky phosphine and substituents on olefin would make the olefin complex and the ethyl complex less stable. This would result in the decrease in exothermicity in the olefin coordination and the decrease in activation barrier for alkane reductive elimination. Steric hindrance would also interrupt an olefin coordination prior to $H_2$ oxidative addition.

Scheme V

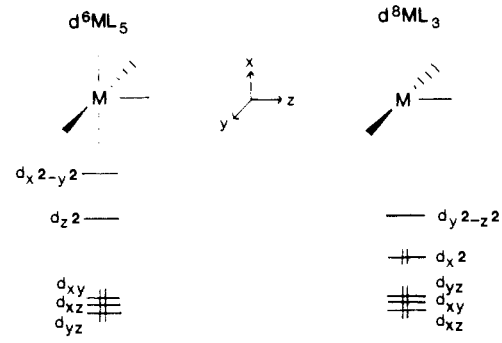


We have also neglected the effect of the solvent completely in the present study. The Halpern mechanism in Scheme I considers the coordination of the solvent S in low coordinate intermediates such as **1**, **2**, and **5**. Very simple minded, one might guess that the solvation would uniformly lower the potential energy profile in Figure 13 from the intermediate **5** through **1** to the intermediate **2**. This would result in the increase in the exothermicity in the isomerization step and the decrease in the exothermicity in the olefin coordination step. This would not change the overall characteristics of the potential energy profile, in particular, in the rate-determining step. A preliminary calculation with a solvent molecule suggests that the situation may not be so simple. Unfortunately, the catalytic system with a solvent molecule or molecules is too large for extensive theoretical studies at the moment and has to be left to a future study.

As the first theoretical study of the full catalytic cycle, we have limited ourselves to the Halpern mechanism of the Wilkinson hydrogenation catalytic cycle. We have essentially followed the intermediates proposed in the mechanism and found that the proposed mechanism is reasonable from the point of view of the theoretical potential energy profile. We also proposed a modification of the mechanism, by indicating that the isomerization of the ethyl hydride complex is an important step in the mechanism. However, we have not examined other alternative pathways proposed by others nor any new alternatives, except for a small study above on the unsaturated mechanism. We feel that in the future this kind of search of alternative pathways can actually be done efficiently by MO theoretical calculations.

In particular, a recent NMR magnetic transfer experiment and molecular modelling study has suggested that the two phosphines are cis in the intermediates when the olefin is bulky as in norbornene and cyclohexene.[47] We do not see any obvious cause of major changes in the potential energy profile upon going from trans to cis complexes, except for the possible unnecessity of the isomerization step. A calculation of cis intermediates and transition states is now in progress.

## IX. Discussions and Comparison with Other Metals

In this section, we will present some additional discussions on the present catalytic system. We will also perform a comparison of the present potential energy profile with those of different metals, in particular, of Pt and Pd, in order to provide a further insight into the nature of reaction and role of metals.

**1. Y-Shape versus T-Shape of 5-Coordinate Complexes.** We have determined the structures of many stationary points of 5-coordinate complexes both as intermediates and as transition states. While all the transition states for oxidative addition of $H_2$, isomerization of ethyl hydride complexes, and reductive elimination are Y-shaped, all the equilibrium structures except for that of $H_2RhCl(PH_3)_2$ are T-shaped.

The transition-metal complex of $d^6$ $ML_5$ type is similar in its electronic structure to that of $d^8$ $ML_3$ type, since both complexes have two d electrons and two d orbitals (yz and $z^2$ or $y^2$-$z^2$) within the molecular plane, the plane containing the metal, the vacant

(47) Brown, J. M.; Evans, P. L.; Lucy, A. R. *J. Chem. Soc., Perkin Trans. II* **1987**, 1589.

Scheme VI

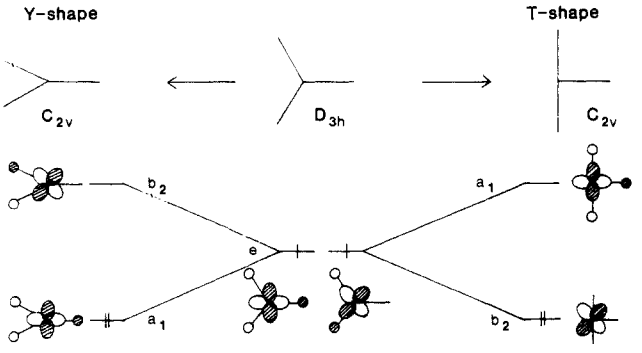


Scheme VII

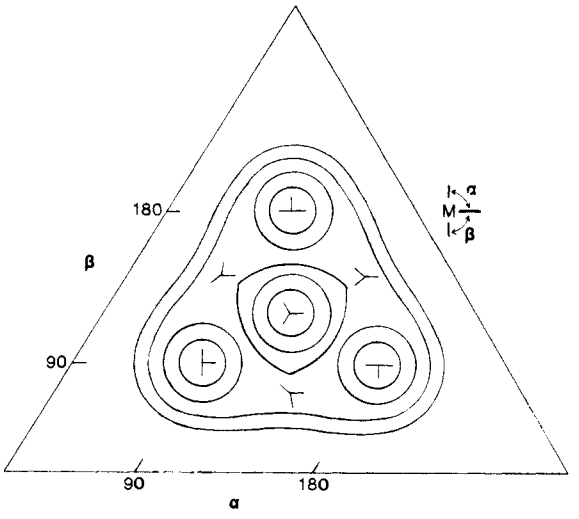


site, and three of the ligands, as shown in Scheme V. If we assume the highly symmetric $D_{3h}$ structure of $d^8$ $ML_3$, the two orbitals in Scheme VI are degenerate and the Jahn–Teller distortion takes place to lead to a T- or a Y-shaped structure. In Scheme VII is shown the schematic potential energy surface of such a system with T-shaped minima connected by Y-shaped transition states. The center of the surface is high in energy due to the Jahn–Teller instability. The structure of $d^8$ $ML_3$ complexes has been studied by the extended Hückel MO method for $Pd(CH_3)_2(PH_3)$ and $Au(CH_3)_3^+$.[43] Tatsumi et al. have proposed that the most stable structures of $PdD_3$, $PdD_2A$, and $PdDA_2$ are T-, Y-, and T-shaped, respectively, in which A is a poor donor ligand and D is a strong donor ligand.[43b] The potential surface for $PdH_3^-$ calculated with the extended Hückel method is like that in Scheme VII.

The potential energy surface of $d^6$ $ML_5$ would be similar, the high-energy center of the potential surface being surrounded by T- and Y-shaped structures. Which of the T- and the Y-shaped structure is more stable may be explained by looking at the relative stability of the two orbitals that are degenerate in the $D_{3h}$ structure. At the Y-shaped structure, one of the degenerate orbitals ($a_1$) goes down in energy to be occupied, while the other is empty. On the other hand, when the structure deforms to a T-shape, the other orbital ($b_2$) becomes occupied.

Let us start this discussion with $H_3Rh(PH_3)_2$, in which the weaker $PH_3$ ligands occupy the trans position, leaving three stronger hydrides in the equatorial position, analogous to $PdH_3^-$. It is expected that the $a_1$ orbital of the Y-shaped structure is less stable than the $b_2$ orbital of the T-shaped structure, because the former mixes with the hydride 1s orbital in an antibonding manner and is destabilized strongly, while the latter is unable to mix with the hydride orbital by symmetry and remains a pure d-orbital, not destabilized, as shown in Scheme VIIIa. Therefore, the T-shaped structures are more stable and local minima.

Replacement of H by Cl changes the potential energy surface. The minimum of $H_2RhCl(PH_3)_2$ (**2**) is Y-shaped, as shown in Figure 1. We also determined the T-shaped structure of **2** shown

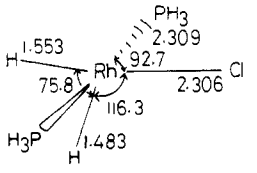


**Figure 14.** The optimized geometry (Å and deg) of $H_2RhCl(PH_3)_2$ under the constraint that the $PH_3$ rotation is frozen at one of the HPRhCl dihedral angles of 90°.

Scheme VIII

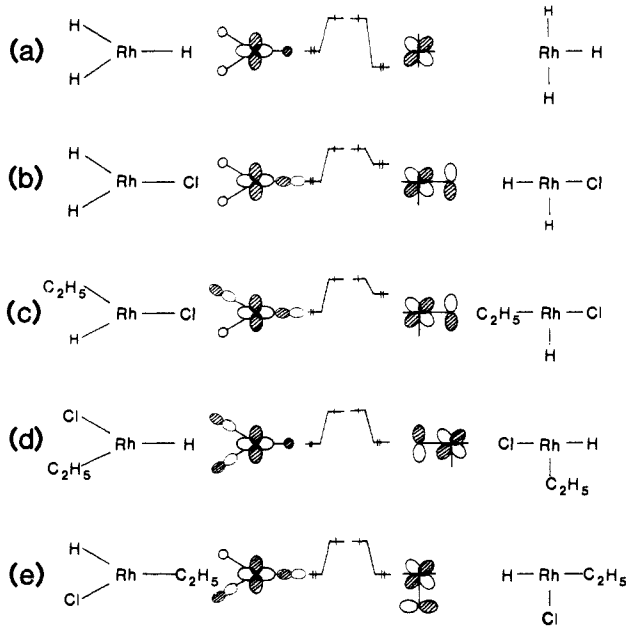


in Figure 14 with the $PH_3$ rotation being frozen at one of the HPRhCl dihedral angles of 90°. If the complex is Y-shaped, the PH bonds and the RhH bonds would be eclipsed. This T-shaped structure is a result of the repulsion between them and is less stable than the Y-shaped structure by only 0.4 kcal/mol, indicating that the potential surface is very flat. This flatness is caused by the chlorine ligand, since $H_3Rh(PH_3)_2$ is T-shaped.

What is the difference between the trihydride and the dihydride chloride complex? In the orbital $b_2$ of T-shaped **2**, the repulsion between the $p\pi$ lone pair of Cl and the metal $d_{yz}$ orbital takes place, while in the Y-shaped complex the difference in symmetry between the $d_{yz}$ metal orbital ($a_1$) and the Cl $p\pi$ lone pair ($b_2$) prevents this destabilization, as shown in Scheme VIII. In addition, the electronegative Cl makes the $a_1$ orbital more stable than in the trihydride complex by a $\sigma$-inductive effect. These effects make the $a_1$ orbital lower in energy in **2**, and therefore the Y-shaped structure is more stable than the T-shaped structure, although the energy difference is only 0.4 kcal/mol.

In Figure 12 we have shown the schematic potential surface of $HRhCl(PH_3)_2(C_2H_5)$. There are three T-shaped equilibrium structures and three Y-shaped transition states, the situation similar to that of $H_3Rh(PH_3)_2$ rather than $H_2RhCl(PH_3)_2$. The Y-shaped structure, TSAB, the analogue of **2**, is not a minimum but a transition state with the activation barrier of around 3 kcal/mol. Steric repulsion between hydride and ethyl seems to make the Y-shaped structure unstable. A strong antibonding interaction between Rh and H and between Rh and $C_2H_5$ makes TSA and TSB, respectively, even less stable. At the Cl-migration transition state, TSAB, this destabilization of the occupied orbital does not take place as was discussed above for $H_2RhCl(PH_3)_2$. This is probably why the Cl migration is the most favorable among Cl, H, and $C_2H_5$ migrations. A high activation energy of $C_2H_5$ migration may be ascribed to the directionality of the $sp^3$ hydride orbital which leads to the less favorable orbital interaction and the strong repulsive interaction between $C_2H_5$ and Rh.

**2. Energy Decomposition Analysis for Comparison between Rh and Pt Complexes in $H_2$ Oxidative Addition and Ethane Reductive**

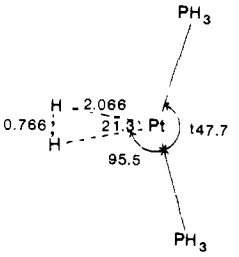


**Figure 15.** The fully optimized geometry (Å and deg) of the transition state for $H_2$ oxidative addition to $Pt(PH_3)_2$.[12a,b]

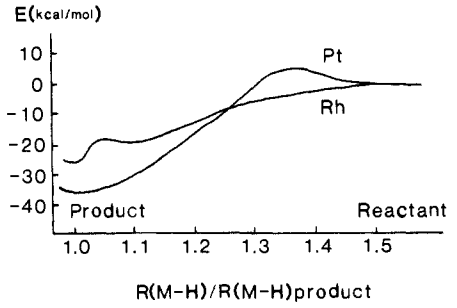


**Figure 16.** Schematic potential energy curves for $H_2$ oxidative addition to $RhCl(PH_3)_2$ and $Pt(PH_3)_2$.

**Elimination.** Here we compare the transition state of $H_2$ oxidative addition of $RhCl(PH_3)_2$ with that of $Pt(PH_3)_2$.[12a,b] The transition-state geometry for $Pt(PH_3)_2 + H_2$ is shown in Figure 15 for comparison with that for $RhCl(PH_3)_2 + H_2$ in Figure 1. Both transition states have a $C_{2v}$ symmetry, though $H_2$ is coplanar with the PMP plane for Pt, while it is perpendicular for Rh. The potential energy curves as functions of the M–H distance are shown in Figure 16. The transition state of the Pt reaction, where the M–H and the H–H distances are 2.07 and 0.77 Å, respectively, is much earlier than that of the Rh reaction where they are 1.57 and 1.03 Å, respectively. The Pt reaction requires a substantial activation barrier of about 5 kcal/mol at the RHF level of calculation, while the Rh reaction takes place virtually with no barrier. In order to clarify these differences between the Rh and the Pt reaction, we have carried out an energy decomposition analysis (EDA)[48] for the energy difference for $Pt(PH_3)_2 + H_2$ between the transition state and the reactants and for $RhCl(PH_3)_2 + H_2$ between the "assumed" transition state (with the Rh–H distance of 2.07 Å and the H–H bond length of 0.77 Å, corresponding to the values at the Pt transition state) and the reactants as well as between the true transition state and the reactants.

In the EDA, the interaction energy is decomposed into the deformation energy of the fragments from their equilibrium geometries and the electronic interaction energy between the deformed fragments. The latter is further divided into the sum of electrostatic and exchange interaction (ES + EX), the electron donative or forward charge-transfer interaction FCTPLX, the back-donative or backward charge-transfer interaction BCTPLX, and the residual higher order interaction. The results are shown in Table V. Every energy component at the transition state is larger for the Rh reaction reflecting its lateness. In order to clarify the difference between the Rh and the Pt reaction, it is more instructive to compare the two systems at the "same" geometry, the true transition state for Pt, and the "assumed" transition state for Rh, as is shown in the last two columns of Table V.

Here the largest difference between Rh and Pt originates from the sum of electrostatic interaction and exchange repulsion. The present three-coordinate Rh complex is formally $d^8$, electron-deficient around the empty coordination site where the low-lying unoccupied d orbital extends as was shown in Figure 3. The approach of $H_2$ toward this site suffers from little exchange repulsion.

**Table V.** Energy Decomposition Analysis of the Energy Difference between the Transition State and the Reactants for Oxidative Addition of $H_2$ to $RhCl(PH_3)_2$ and $Pt(PH_3)_2$ (kcal/mol)

| | Rh | | | |
|---|---|---|---|---|
| | $H_2$ complex | TS | assumed TS[a] | Pt[c] |
| deformation | | | | |
| metal fragment[b] | −0.7 (0.1) | −0.5 (0.2) | 0.0 (0.8) | 3.1 |
| $H_2$ | 5.9 | 23.6 | 0.3 | 0.3 |
| sum | 5.2 | 23.1 | 0.3 | 3.4 |
| interaction | | | | |
| ES + EX | 43.0 | 69.7 | 1.6 | 16.9 |
| BCTPLX | −24.3 | −42.6 | −4.8 | −7.2 |
| FCTPLX | −44.0 | −68.8 | −7.5 | −10.7 |
| residue | 0.0 | −0.9 | −0.9 | 2.8 |
| sum | −25.3 | −42.6 | −11.6 | 1.8 |
| total | −20.1 | −19.5 | −11.2 | 5.2 |

[a] The Rh–H distance of 2.07 Å and the H–H bond length of 0.77 Å are taken from the transition state for the Pt system, but all the other geometrical parameters are those of the true TS. [b] Relative to the $C_s$ structure of $RhCl(PH_3)_2$ (**1**). Numbers in parentheses are relative to the true $C_{2v}$ minimum energy structure. [c] Reference 12b.

At the same time, the unoccupied d orbital that extends to the empty coordination site provides a favorable donative interaction FCTPLX. Both of these interactions, (ES + EX) and FCTPLX, as well as the Rh d → $H_2$ $\sigma^*$ back-donative interaction BCTPLX, are attractive and occur without deformation of the reactant geometries. Thus the formation of the weak $H_2$ complex does not require any activation barrier. In this $H_2$ complex, the H–H bond has already been activated mainly by the donative interaction, and the stretching of the H–H bond to reach the transition state results in only a very small increase in the total energy, i.e., a small activation energy, if any.

Table V indicates also that the transition state for $Pt(PH_3)_2$ suffers from a large ES + EX repulsion. $Pt(PH_3)_2$ is formally $d^{10}$ and all the d orbitals are occupied. The incoming $H_2$ feels a strong exchange repulsive interaction in the early stage of reaction. One also notices that there is a substantial deformation energy of the metal fragment in this early transition state. This deformation energy comes mainly from P–Pt–P bending from the linearity. This bending is required to make the occupied $d_{xy}$ orbital higher in energy to assist $\pi$ back-donative interaction as well as to make the unoccupied sp hybrid orbital extend out to the empty coordination site for better donative interaction.[49]

Once the transition state is passed, the potential energy profile for Pt crosses that for Rh and results in a larger exothermicity than Rh. This larger exothermicity is, as will be discussed in the next subsection, due to the binding energy of the Pt–H bond which is larger than that of the Rh–H bond.

Obara et al. have also studied the reductive elimination of $CH_4$ from $HPt(PH_3)_2(CH_3)$,[12b] to find a much larger activation barrier of 38 kcal/mol at the HF level of calculation, compared with 14 kcal/mol of the present reductive elimination of $C_2H_6$ from $HRhCl(PH_3)_2(C_2H_5)$. This difference can be explained similarly to the difference in the $H_2$ oxidative addition between Rh and Pt. The barrier height for the reductive elimination is the sum of the barrier height and the exothermicity of the oxidative addition, the reverse reaction. The higher reductive elimination barrier for Pt than for Rh can be attributed to two factors. The Pt–C and Pt–H bonds are stronger than the Rh–C and Rh–H bonds, respectively, and therefore, it requires a larger energy to reach the transition state for Pt than for Rh. At the transition state the exchange repulsion between the partly formed CH bond and the fully occupied d orbitals is larger for Pt. In addition, the Rh reaction is promoted further by the charge-transfer interaction

(48) (a) Morokuma, K.; Kitaura, K. *Chemical Application of Atomic and Molecular Electrostatic Potentials*; Politzer, P., Truhler, D. G., Eds.; Plenum: New York, 1981. (b) Kitaura, K.; Sakaki, S.; Morokuma, K. *Inorg. Chem.* **1981**, *20*, 2292.

(49) The magnitude of the donative interaction FCTPLX at the Pt transition sate is larger than that at the Rh "assumed" transition state. Several factors may contribute to this unrealistic result. One might blame in part the inadequacy of the Pt ECP parameters used in this calculation that tend to make Pt–ligand bonds stronger than real.[12c]

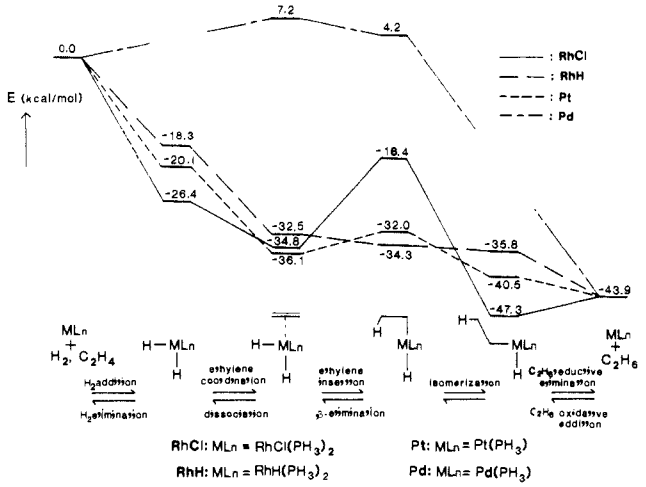


**Figure 17.** Energy changes of the full hydrogenation cycle of **RhCl**, **RhH**, **Pt**, and **Pd** in kcal/mol. The profiles show only the energies of intermediates and do not show those of transition states connecting them.

from the CH bond to a low-lying unoccupied d orbital.

**3. Comparison of Olefin Insertion between $RhCl(PH_3)_2$ and $RhH(PH_3)_2$, $PtPH_3$, and $PdPH_3$.** The facts that the olefin insertion is rate-determining and that its reverse reaction is prohibitive due to a high activation barrier are essential features of the olefin hydrogenation by the Wilkinson catalyst, where olefin isomerization does not take place. This olefin insertion is different from that of the group 10 transition-metal complexes we have previously studied.[13]

$$H_2M(C_2H_4)(PH_3) \rightarrow HM(C_2H_5)(PH_3) \qquad (M = Pd, Pt)$$

The Pd and Pt reactions are nearly thermoneutral, i.e., exothermic by 3.0 kcal/mol and endothermic by 4.2 kcal/mol, respectively, at the HF level, while the present olefin insertion of Rh is very *endothermic* (16.4 kcal/mol). In addition, the activation barrier of the Pd and Pt reactions (8.0 and 12.5 kcal/mol, respectively) is lower than that of the Rh reaction (18.4 kcal/mol). We also notice that the effect of Cl on this endothermicity is phenomenal. The olefin insertion of $H_3Rh(PH_3)_2(C_2H_4)$, in which Cl in **3** is replaced by H, is calculated to be *exothermic* by 1.8 kcal/mol.

In the present subsection, we will concentrate on the effect of the transition metals and the non-reactive ligand Cl on the catalytic cycle. To carry out a systematic study, we have optimized the structures of model catalysts $ML_n$, i.e., $RhH(PH_3)_2$, $Pd(PH_3)$, $Pt(PH_3)$ as well as $RhCl(PH_3)_2$ (referred to as **RhH**, **Pd**, **Pt**, and **RhCl**, respectively, in this subsection) and intermediates derivable from them, $H_2$ and $C_2H_4$. $RhH(PH_3)_2$ is an assumed hydride complex used to examine the effect of the Cl ligand.

In Figure 17 are shown the energy profiles (relative to $ML_n + H_2 + C_2H_4$). Note that these profiles depict only the energies of intermediates and provide no information on the activation barriers between them. One can see some differences and similarities between the model Wilkinson system (**RhCl**) and the others. The largest difference is in the olefin insertion, as was discussed above.

In order to clarify the origin of this difference, we have estimated the binding energies between the metal and the ligands, $C_2H_4$, $C_2H_5$, and H, as functions of the metal and the other neighboring ligands. For this purpose, we at first consider a formal network of chemical processes shown in Scheme IX and calculate for each process the energy difference, $\Delta E$, which is negative when the corresponding process is exothermic. All the structures of intermediates are optimized.[50] Although E and K are symmetry-forbidden, it is still possible to formally calculate the energy difference of the processes. The catalytic cycle corresponds to the sequence A, B, and C, followed by the isomerization of the ethyl complex. The final step is process H or L. The energy changes, $\Delta E$, of the processes shown in Table VI are related to the binding energies, D, as follows:

A: $2D(M-H) - D(H-H) = -\Delta E(A)$

B: $D(M-C_2H_4) = -\Delta E(B)$

C: $D(M-C_2H_5) - D(M-H) - D(M-C_2H_4) + D(C-H) - D(C=C) = -\Delta E(C)$

D: $D(C_2H_5-H) - D(M-C_2H_5) - D(M-H) = -\Delta E(D)$

E: $2D(M-H) - D(H-H) = -\Delta E(E)$

F: $D(M-C_2H_4) = -\Delta E(F)$

G: $D(M-C_2H_5) - D(M-H) - D(M-C_2H_4) + D(C-H) - D(C=C) = -\Delta E(G)$

H: $D(C_2H_5-H) - D(M-C_2H_5) - D(M-H) = -\Delta E(H)$

I: $D(M-C_2H_4) = -\Delta E(I)$

J: $2D(M-H) - D(H-H) = -\Delta E(J)$

K: $2D(M-H) - D(H-H) = -\Delta E(K)$

L: $D(C_2H_2-H) - D(M-C_2H_2) - D(M-H) = -\Delta E(L)$

Here $D(C{=}C)$ refers to the binding energy only due to the $\pi$ electrons. Though the binding energies thus calculated represent the strengths of the corresponding bonds, they obviously include implicitly the effects of neighboring bonds which are neither broken nor created. Of course, these values based on the HF (ROHF for free radical intermediates) calculation should be taken to be qualitative, but still provide a guide to the different behavior of potential profiles.

**Table VI.** Energy Changes, $-\Delta E$, of Model Processes Used for Calculation of Differences in Bond Strength (kcal/mol)[a]

| | RhCl | RhH | Pd | Pt |
|---|---|---|---|---|
| A | 26.4 | 16.3 | | 20.1 |
| B | 8.4 | 16.3 | | 16.0 |
| C | −16.4 | 1.8 | 3.0 | −4.1 |
| D | 25.5 | 9.6 | 48.1 | 11.9 |
| E | −11.7 | 16.3 | −21.1 | 13.6 |
| F | 29.0 | 16.3 | | 22.4 |
| G | 30.1 | 1.8 | | |
| H | −3.4 | 8.3 | | 3.5 |
| I | 34.7 | 21.3 | | 22.5 |
| J | 0.1 | 11.2 | | 13.6 |
| K | −17.4 | 11.2 | | 13.4 |
| L | −0.9 | 12.4 | | |

[a] Energies at the HF level at the HF optimized geometries. The corresponding binding energies for H–H and H–$C_2H_5$ are 81.9 and 86.3 kcal/mol, respectively.

**Table VII.** Estimated Rh–$C_2H_4$ Binding Energy (kcal/mol) as a Function of Other Ligands

| | cis ligands | | |
|---|---|---|---|
| trans ligand | v[a] v | H H | H Cl |
| H | 21.3 (I)[b] | 16.3 (B, F) | 8.4 (B) |
| Cl | 34.7 (I) | 29.0 (F) | |

[a] v stands for a vacant coordination site. [b] The symbol in parentheses corresponds to the process in Scheme IX and Table VI, for which the binding energy was calculated.

**(i) Comparison of the Olefin Insertion between $RhCl(PH_3)_2$ and $RhH(PH_3)_2$, Chloride versus Hydride.** First, let us focus on the Rh–$C_2H_4$ bond. The binding energies $D(M-C_2H_4)$ calculated from the processes B, F, and I given in Table VII show their variations depending on the trans and cis ligands. In Table VII, for instance, 21.3 kcal/mol is taken from processes I for **RhH** in Table VI, where ethylene has two vacant cis sites (v v) and a *trans*-H ligand, in addition to two common *cis*-$PH_3$'s. The trans H ligand makes the Rh–$C_2H_4$ bond weaker by 13.1 kcal/mol, an average of (34.7 − 21.3) and (29.0 − 16.3), than the *trans*-Cl

(50) For Pt we used valence double-$\zeta$ basis functions of Noell and Hay[50a] with the relativistic effective core potential, the 3-21G[22] for $C_2H_4$, $C_2H_5$, and hydride and the STO-2G[23] for $PH_3$. (a) Noell, J. O.; Hay, P. J. *Inorg. Chem.* **1982**, *21*, 14.

Scheme IX

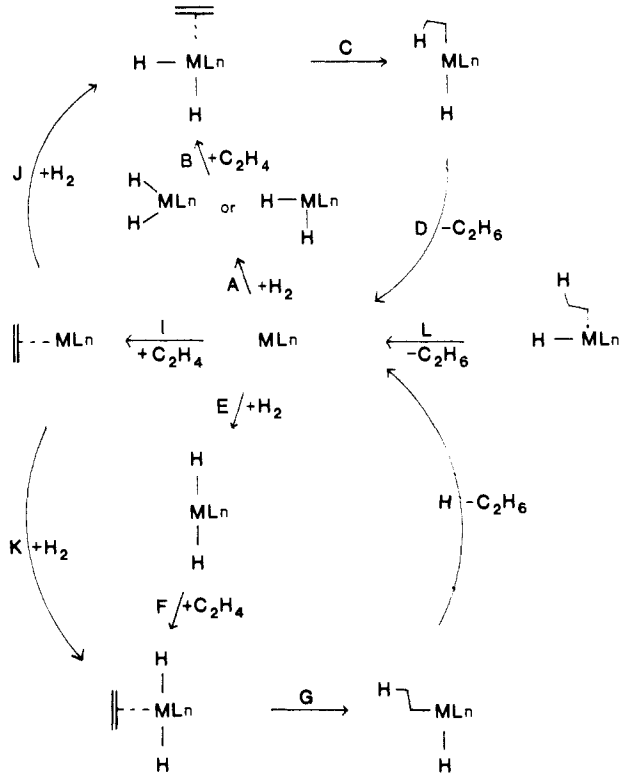


Table VIII. Estimated Rh–H Binding Energies (kcal/mol) as a Function of Other Ligands[a]

| | cis ligand | |
|---|---|---|
| cis ligand | H | Cl |
| v[b] | 49.1 (E)[c] | 35.1 (E) |
| $C_2H_4$ | 46.6 (K) | 32.3 (K) |

[a] The trans ligand is H. [b,c] See footnotes of Table VII.

ligand, indicating that the trans effect is larger in H than in Cl. On the other hand, the *cis*-H makes the Rh–$C_2H_4$ bond weaker by 2.7 kcal/mol per one *cis*-H, an average of (21.3 – 16.3)/2 and (34.7 – 29.0)/2, compared with the vacant site. A *cis*-Cl leads to a weaker Rh–$C_2H_4$ bond by 7.9 kcal/mol (16.3 – 8.4) than a *cis*-H and thus by 10.6 kcal/mol than a vacant site. This *cis*-Cl effect has been discussed also in preceding sections.

Next, the Rh–H binding energies are calculated from processes E and K as shown in Table VIII. For instance 49.1 kcal/mol is obtained as (16.3 + 81.9)/2, where 81.9 kcal/mol is the calculated H–H binding energy in $H_2$. The Rh–H bond cis to Cl is weaker than that cis to H by 14.2 kcal/mol, an average of (49.1 – 35.1) and (46.6 – 32.3). This is the *cis*-Cl effect on the Rh–H bond, which is again very large. The *cis*-$C_2H_4$ coordination weakens (relative to the vacant site) the Rh–H bond by 2.7 kcal/mol, an average of (32.3 – 35.1) and (46.6 – 49.1).

The sum of the Rh–$C_2H_5$ and the Rh–H binding energy may be estimated, as shown in Table IX, using processes L, D, and H, where the two bonds concerned are located cis, trans, and cis with respect to each other, respectively. In Table IX, for instance, 87.2 kcal/mol is calculated as 86.3 – (–0.9) from Table VI. Using the values in Table IX and the *cis*-Cl effect (relative to H) on the Rh–H bond, 14.2 kcal/mol, obtained above, one can estimate the Rh–$C_2H_5$ binding energy differences. The *cis*-H effect can be estimated by using process D that the Rh–$C_2H_5$ bond cis to H is 1.7 kcal/mol (76.7 – 60.8 – 14.2) stronger than that cis to Cl. This, however, includes the difference in the agostic interaction caused by the Cl trans effect on the Rh···HC interaction. The agostic interaction was estimated in Section V to make the eclipsed conformation, **4**, lower in energy by 3.5 kcal/mol than the staggered conformation, while the replacement of Cl by H weakens

Table IX. Sum of Estimated Rh–$C_2H_5$ and Rh–H Binding Energies as a Function of Other Ligands (kcal/mol)

| Rh–H | | Rh–$C_2H_5$ | |
|---|---|---|---|
| cis Et v[a]<br>trans Cl | + | cis H Cl<br>trans v | 87.2 (L)[b] |
| cis Et v<br>trans H | + | cis H H<br>trans v | 73.9 (L) |
| cis Et Cl<br>trans v | + | cis v H<br>trans Cl | 89.7 (H) |
| cis Et H<br>trans v | + | cis v H<br>trans H | 78.0 (H) |
| cis v Cl<br>trans Et | + | cis v Cl<br>trans H | 60.8 (D) |
| cis v H<br>trans Et | + | cis v H<br>trans H | 76.7 (D) |

[a,b] See footnotes for Table VII.

Table X. Estimated Relative Trans and Cis Effects Summarized (kcal/mol)

| | | cis | | trans |
|---|---|---|---|---|
| Rh–$C_2H_4$ | H → v | 2.7 | H → Cl | 13.1 |
| | Cl → H | 7.9 | | |
| Rh–H | Cl → H | 14.2 | H → Cl | 19.8 |
| | $C_2H_4$ → v | 2.7 | | |
| Rh–$C_2H_5$ | Cl → H | 6.5 | H → Cl | 25.9 |

the agostic interaction due to the stronger H trans effect, so that the eclipsed conformation of $H_2Rh(PH_3)_2(C_2H_5)$ becomes less stable than the staggered conformation by 1.3 kcal/mol. The difference in the agostic interaction is thus 4.8 kcal/mol, which strengthens the Rh–$C_2H_5$ bond in **RhCl**. Therefore, the Cl cis effect (relative to H) on the Rh–$C_2H_5$ bond is estimated to be 6.5 kcal/mol (1.7 + 4.8). On the other hand, the trans effect on the Rh–$C_2H_5$ bond can be estimated by using process H (Table IX). Using again the *cis*-Cl effect on the Rh–H bond (14.2 kcal/mol), one finds that the *trans*-H effect makes the Rh–$C_2H_5$ bond weaker by 25.9 kcal/mol (89.7 – 78.0 + 14.2) than the *trans*-Cl effect.

Finally the trans effect on the Rh–H bond can be estimated by looking at process L and the above obtained *cis*-Cl effect 6.5 kcal/mol relative to *cis*-H; a *trans*-H leads to weaker Rh–H bonding than a *trans*-Cl by 19.8 kcal/mol (87.2 – 73.9 + 6.5).

The above results are summarized in Table X. For instance, the *cis*-Cl has a larger cis effect on the Rh–H bond, i.e., makes the bond weaker, by 14.2 kcal/mol than the *cis*-H. Now, we can discuss the difference in endothermicity for olefin insertion between **RhH** and **RhCl** as well as for other steps of the catalytic cycle. First, we pay attention to the rate-determining olefin insertion. The reaction of **RhCl** is more endothermic by 18.2 kcal/mol than that of **RhH**, as is shown for process C in Table VI. The present estimation of binding energy differences gives the endothermicity difference of 18.4 kcal/mol (19.8 – 7.9 + 6.5), in good agreement with this value. This estimation reveals that the Rh–H bond to be broken in **RhCl** is stronger (by 19.8 kcal/mol) than that in **RhH** due to the weaker trans effect of Cl than H, while the ligand effect on M–$C_2H_4$ and M–$C_2H_5$ is nearly canceled. This is the reason why the olefin insertion requires a much higher activation barrier to become the rate-determining step. Figure 17 shows that this difference in the endothermicity mainly comes from the difference in the *trans*-ethyl hydride complex. In this complex, both the Rh–H and the Rh–$C_2H_5$ bonds are much weaker for **RhCl** (relative to **RhH**) due to the strong *cis*-Cl effect. One sees clearly the *cis*-Cl effect plays a key role in making this step rate-determining.

Other features of the potential surface of **RhCl** compared with that of **RhH** can be also understood by using the above estimation of binding energies. The $H_2$ oxidative addition of **RhH** is less exothermic by 10.1 kcal/mol (cf. Figure 17 and process A of Table VI). Since the dihydride complexes of **RhCl** and **RhH** are Y- and T-shaped, respectively, a direct comparison between them is not

Table XI. Binding Energies in Pd and Pt Complexes (kcal/mol)

| bond | binding energy Pd | binding energy Pt | trans ligand |
|---|---|---|---|
| $M-C_2H_4$ | | 22.5 (I)[a] | $PH_3$ |
| | | 22.4 (F) | $PH_3$ |
| | | 16.0 (B) | H |
| M–H | | 51.0 (A) | |
| | 30.4 | 47.8 (E) | H |
| | | 47.7 (K) | H |
| $M-H + M-C_2H_5$ | 38.2 | 74.4 (D) | |

[a] See footnotes for Table VII.

possible. However, it is fair to say that, compared with **RhCl**, the strong *trans*-H effect in **RhH** makes the Rh–H bond weaker (by 19.8 kcal/mol), which in turn makes the $H_2$ addition reaction less exothermic. The smaller exothermicity in olefin coordination of **RhCl** (by 7.9 kcal/mol) is ascribable to the *cis*-Cl effect (by 7.9 kcal/mol) on the $Rh-C_2H_4$ binding energy.

The $C_2H_6$ reductive elimination for **RhCl** is almost thermoneutral, while that for **RhH** is exothermic. The nonleaving X (=H or Cl) in any of the *cis*-ethyl hydride complexes always has one of the leaving groups, H or $C_2H_5$, cis and the other at the trans position. The *trans*-H effect is larger than the *cis*-Cl effect (cf. Table X), dominating the scene to make the elimination of $C_2H_6$ more exothermic in **RhH** than in **RhCl**.

**(ii) Comparison among Rh, Pd, and Pt.** Various binding energies calculated for **Pd** and **Pt** are shown in Table XI. As seen in Figure 17, the ethylene dihydride and ethyl hydride Pd complexes are much higher in energy than the others, i.e., the oxidative addition of $H_2$ and $C_2H_6$ to the $Pd(PH_3)$ is very endothermic, in agreement with the theoretical studies done by Low and Goddard,[12c,d,e] who have discussed the difference in oxidative addition/reductive elimination between the Pd and the Pt complex. This large endothermicity is due to the weak Pd–H and Pd–C bonds. $D(M-H) + D(M-C_2H_5)$ obtained from process D are 60.8, 76.7, 74.4, and 38.2 kcal/mol for **RhCl**, **RhH**, **Pt**, and **Pd**, respectively (cf. Table XI as well as Table IX). The difference between **Pd** and **Pt** (36.2 kcal/mol) agrees qualitatively with our previous result of 27.8 kcal/mol in carbonyl insertion reaction.[14c] It is clear that the high energy of the intermediates makes the **Pd** system unfavorable as a catalyst.

The **Pt** potential energy profile is similar in nature to the **RhH** profile. For **Pt**, the $H_2$ oxidative addition (process A), the ethylene coordination (B), and the $C_2H_6$ reductive elimination (D) are exothermic by 20.1, 16.0, and 3.4 kcal/mol, respectively, while the corresponding processes for **RhH** are exothermic by 16.3, 16.2, and 8.3 kcal/mol, respectively. A slightly larger difference is found in the olefin insertion (process C): endothermic by 4.1 kcal/mol for **Pt** and exothermic by 1.9 kcal/mol for **RhH**. The binding energies of $Pt-C_2H_4$, Pt–H, and $(Pt-H) + (Pt-C_2H_5)$ shown in Table XI are close to those for **RhH**.

Finally we would like to compare the potential energy profile between the **RhCl** and the **Pt** catalytic system. In the olefin insertion step, the **RhCl** system has to reach the unstable *trans*-ethyl hydride complex from the ethylene dihydride complex very endothermically, before isomerizing very exothermically to a *cis*-ethyl hydride complex. The reverse $\beta$-elimination from a stable *cis*-ethyl hydride complex, therefore, requires a high activation energy, e.g., 30.9 kcal/mol from **5A** to **4**. This barrier is higher than that for the final catalytic step of reductive elimination. Therefore, the reverse reaction would not take place and there would be no olefin isomerization via a series of olefin insertion and $\beta$-elimination. This is an important requirement for a practical catalyst.

On the other hand, in the catalytic cycle of **Pt**, both *trans*- and *cis*-ethyl hydride complexes are similar in energy to the ethylene dihydride complex. Therefore, the activation barriers for the nearly thermoneutral olefin insertion and for the trans $\leftrightarrow$ cis isomerization processes for **Pt** are expected to be lower than those for **RhCl**. The barrier for the reverse reaction, $\beta$-elimination, of the *trans*-Pt complex has been calculated to be 7.3 kcal/mol.[13] On the other hand, there is a high activation barrier for alkane reductive elimination from the Pt complex (for instance, 31.7 kcal/mol for $HPt(PH_3)_2(CH_3) \rightarrow Pt(PH_3)_2 + CH_4$ at the HF level).[12b] This high barrier makes the final reductive elimination step hard for the **Pt** catalytic system. Crossing the low-energy $\beta$-elimination and reverse olefin insertion barriers repeatedly, the **Pt** system will probably cause isomerization of olefin, if reactions other than those studied here do not take place. Thus the **Pt** system is not a good hydrogenation catalyst, because of the high activation barrier for reductive elimination and the low activation barrier for the cis–trans olefin isomerization. The former difficulty could be overcome by high pressure and high temperature. The ethylene hydrogenation by $PtH_2(P\text{-}t\text{-}Bu_2(CH_2)_3P\text{-}t\text{-}Bu_2)$ under such a condition may be an example.[28b] The latter could be changed by introducing a ligand with a weak trans effect. This would make the trans intermediate unstable and the barrier higher.

## X. Concluding Remarks

An extensive use of the ab initio MO method with the energy gradient has clarified the potential energy profile for the full catalytic cycle of ethylene hydrogenation by $RhCl(PH_3)_2$, the model Wilkinson olefin hydrogenation catalytic cycle following the Halpern mechanism. The profile of the full cycle consisting of the oxidative addition of $H_2$, the ethylene coordination, the intramolecular migratory olefin insertion, the isomerization of ethyl hydride complex, and the reductive elimination of $C_2H_6$ has been found to be smooth without excessive barriers and too stable intermediates. The first two reactions are exothermic with little or no activation barrier. Olefin insertion, followed by isomerization of the *trans*-ethyl hydride intermediate to a cis complex through hydrogen and chloride migration, is the rate-determining step with a barrier height of about 20 kcal/mol. These two reactions, exothermic overall, may take place as one combined step with little stability in the trans intermediate. The final step of reductive elimination of $C_2H_6$ from the cis complex is nearly thermoneutral with a modest barrier. These features of the potential energy profile have shown that the Halpern mechanism is favorable.

Comparing the present potential energy profile with that of $RhH(PH_3)_2$, we have found that a chloride and a hydride make the cis and the trans bond weaker, respectively. The Rh–H bond to be broken in the rate-determining olefin insertion of the Wilkinson system is strong due to the weak trans effect of the *trans*-Cl ligand. This makes the barrier of the olefin insertion high and rate-determining.

In the Wilkinson system, the olefin insertion and the following isomerization via hydride migration takes place as one combined step with a high barrier. The reverse reaction, the isomerization to *trans*-ethyl hydride complex and $\beta$-elimination, has a high barrier, higher than that of the final reductive elimination. On the other hand in the Pt complex the activation barrier of the final reductive elimination is high, while that for the reverse reaction of olefin insertion is low, leading to olefin isomerization. The Pt complex is not a good catalyst for hydrogenation.

Though the models used may be oversimplified, we have been able to determine the structures and the energies of the intermediates and transition states of the elementary reactions in a catalytic cycle with the ab initio MO method and obtain the potential energy profile of a full catalytic cycle. Once this is done, it is not very difficult to extend the calculation to different metals and ligands, other than those studied experimentally. Even a catalytic cycle of an unknown complex could be a subject of an ab initio MO study. One may some day be able to use the information obtained from such a study for a theoretical design of a new catalyst.

**Acknowledgment.** The authors are grateful to Professor J. Halpern for stimulating discussions and suggestions and Dr. P. J. Hay and Dr. R. L. Martin for giving the ECP integral code for GAUSSIAN82. All the numerical calculations were carried out at the IMS computer center. C.D. acknowledges a JSPS-CNRS Exchange Scholar award. J.H. and X.Y.F. were Visiting Scientists at IMS, where most of the work was carried out.

**Registry No. 1**, 72152-06-8; $H_2$, 1333-74-0; ethylene, 74-85-1.